Electronic Supplementary Material (ESI) for Polymer Chemistry.

- Electronic Supplementary Information -

Design and mechanical properties of supramolecular polymeric materials based on host-guest interactions: the relation between relaxation time and fracture energy

Subaru Konishi,[a] Yu Kashiwagi,[a] Go Watanabe,[b] Motofumi Osaki,[a,c] Takuya Katashima,[d] Osamu Urakawa,[a] Tadashi Inoue,[a,c] Hiroyasu Yamaguchi,[a,c] Akira Harada,[e] and Yoshinori Takashima*[a,c,f]*

[a] Department of Macromolecular Science, Graduate School of Science, Osaka University.

1-1 Machikaneyama-cho, Toyonaka, Osaka 560-0043 (Japan).

[b] Department of Physics, School of Science, Kitasato University.

1-15-1 Kitasato, Minami-ku, Sagamihara, Kanagawa 252-0373 (Japan).

[c] Project Research Center for Fundamental Sciences, Osaka University,

1-1 Machikaneyama-cho, Toyonaka, Osaka 560-0043 (Japan).

[d] Department of Bioengineering, School of Engineering, The University of Tokyo.

7-3-1 Hongo, Bunkyo-ku, Tokyo 113-8656 (Japan).

[e] The Institute of Scientific and Industrial Research, Osaka University,

8-1 Mihogaoka, Ibaraki, Osaka 567-0047 (Japan).

[f] Institute for Advanced Co-Creation Studies, Osaka University,

2-1 Yamada-oka, Suita, Osaka 565-0871 (Japan).

E-mail: harada@chem.sci.osaka-u.ac.jp

takasima@chem.sci.osaka-u.ac.jp.

Content

Experimental details

Materials

Acrylamide (AAm) and *N*-(hydroxymethyl)acrylamide were purchased from Wako Pure Chemical Industries, Ltd. α-Cyclodextrin (αCD) and β-cyclodextrin (βCD) were obtained from Junsei Chemical Co. Ltd. Acetone, methanol, diethyl ether, ethyl acetate, acrylic acid, hydrochloric acid, sodium hydroxide, sodium sulfate, *p*-toluenesulfonic acid monohydrate, potassium peroxodisulfate (KPS), *N,N,N′,N′*–tetramethylethylenediamine (TEMED), *N,N′*–methylenebis(acrylamide) (MBAAm), 1-methylimidazole and pyridine were purchased from Nacalai Tesque Inc. Dimethyl sulfoxide-d_6 (DMSO–d_6) was obtained from Merck & Co., Inc. Chloroform-*d* ($CDCl_3$) and deuterium oxide (D_2O) were obtained from EURISO-TOP. 4,4'-Bipyridyl and trimethylamine (in acetonitrile) were purchased from Tokyo Kasei. Sodium 3-(trimethylsilyl)-1-propanesulfonate (DSS) was purchased from Sigma-Aldrich. The water used for the preparation of the aqueous solutions was purified with a Millipore Elix 5 system. Other reagents were used without further purification. Acrylamido-methyl ether-modified αCD and βCD (αCDAAmMe and βCDAAmMe) and 4-(11-acryloyloxyundecyl)-4'-(methyl)-bipyridinium dichloride (VC11 monomer) were prepared according to our previous reports.[1,2]

Measurements

^{1}H and ^{13}C nuclear magnetic resonance (NMR) spectroscopy: ^{1}H and ^{13}C NMR spectra were recorded with a JEOL JNM–ECA 400 NMR spectrometer (400 MHz) and a JEOL JNM–ECA 500 NMR spectrometer (500 MHz). Solid–state ^{1}H field gradient magic angle spinning (FG-MAS) NMR spectra were recorded with a JEOL JNM–ECA 400 NMR spectrometer (400 MHz, with a sample spinning rate of 7 kHz). 2-dimentional ^{1}H Rotating-frame Overhauser effect spectroscopy (2D ROESY) NMR spectra were performed at 600 MHz with an Aglient VNS600 NMR spectrometer. All chemical shifts were referenced to the residual solvent peaks as internal standards (for ^{1}H NMR: δ = 0 ppm for tetramethylsilane (TMS), 2.49 ppm for DMSO–d_6, 4.79 ppm for D_2O, and 7.26 ppm for $CDCl_3$, ^{13}C NMR: δ = 0 ppm for TMS and DSS, 39.5 ppm for DMSO–d_6, and 77.0 ppm for $CDCl_3$).

Mass spectroscopy: Matrix-assisted LASER desorption/ionization time-of-flight mass spectrometry (MALDI-TOF MS) was conducted on a Bruker autoflex speed mass spectrometer using 2,5-dihydroxy-benzoic acid as a matrix. Electrospray ionization-linear ion trap-orbitrap (ESI-LIT-orbitrap) mass spectroscopy was conducted on a Thermo Fisher Scientific Orbitrap XL using methanol as solvent.

Fourier-transfrom infrared (FT-IR) spectroscopy: FT-IR spectra were acquired using a JASCO FT/IR–410 spectrometer.

Isothermal titration calorimetry (ITC): ITC measurements were performed by Malvern MicroCal iTC200 system.

Tensile test: Tensile tests were performed on a universal testing machine [Autograph AG-X plus (Shimadzu Co.)] equipped with a 20 N load cell and 1 N clip grips. The hydrogels were prepared using type 3 dumbbell-shaped Teflon mold following the JIS K6251 standard. Based on

the stress-strain curves, fracture strength and strain were defined as the maximum stress and strain before stress decreasing. G_f was calculated from integral of stress-strain curve and the fracture strain was set as the upper limit of the integral. E was calculated from initial slope of stress-strain curve at a range between 3%–8% strain.

Rheological measurement: Dynamic viscoelasticity was measured using an Anton Paar MCR302 rheometer.

2. Preparation of guest monomers

Preparation of 3-(11-acryloyloxyundecyl)-1-methyl-imidazolium bromide (ImC11)

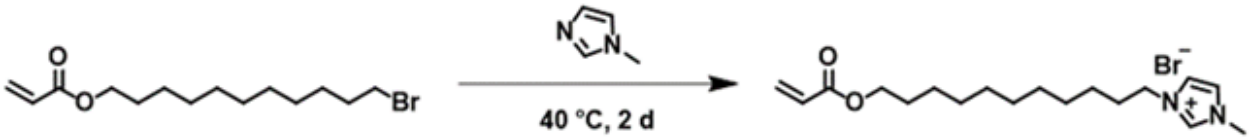

Scheme S1. Preparation of ImC11.

4-(11-Acryloyloxyundecyl)-4'-bipyridinium bromide (5.77 g, 19 mmol) was dissolved in 1-methylimidazole (1.5 mL, 19 mmol), and the solution was stirred for 2 days at 40 °C. The resulting solution was poured into diethyl ether to precipitate the crude product, which was collected by filtration and washed with diethyl ether. ImC11 was obtained as white solid (6.47 g, 88% yield).

^{1}H NMR (400 MHz, D_2O): δ = 8.71 (s, 1H), 7.48 (t, J = 1.6 Hz, 1H), 7.44 (t, J = 1.6 Hz, 1H), 6.43 (dd, J = 17.2, 1.2 Hz, 1H), 6.22 (dd, J = 17.2, 10.4 Hz, 1H), 5.98 (dd, J = 10.4, 1.2 Hz, 1H), 4.24–4.18 (m, 4H), 3.90 (s, 3H), 1.88 (quin, J = 7.2 Hz, 2H), 1.70 (quin, J = 6.8 Hz, 2H), 1.42–1.29 (m, 14H) (see **Figure S1**).

^{13}C NMR (125 MHz, $CDCl_3$): δ = 166.32, 137.69, 130.40, 128.58, 123.34, 121.64, 64.61, 50.15, 37.74, 30.23, 29.31, 29.28, 29.22, 29.08, 28.88, 28.51, 26.18, 25.80 (see **Figure S2**).

ESI-LIT-orbitrap MS: *m*/*z*

Calcd. for $C_{18}H_{31}N_2O_2$ ($[M - Br]^+$): 307.2380;

Found: 307.2378 (see **Figure S3**)

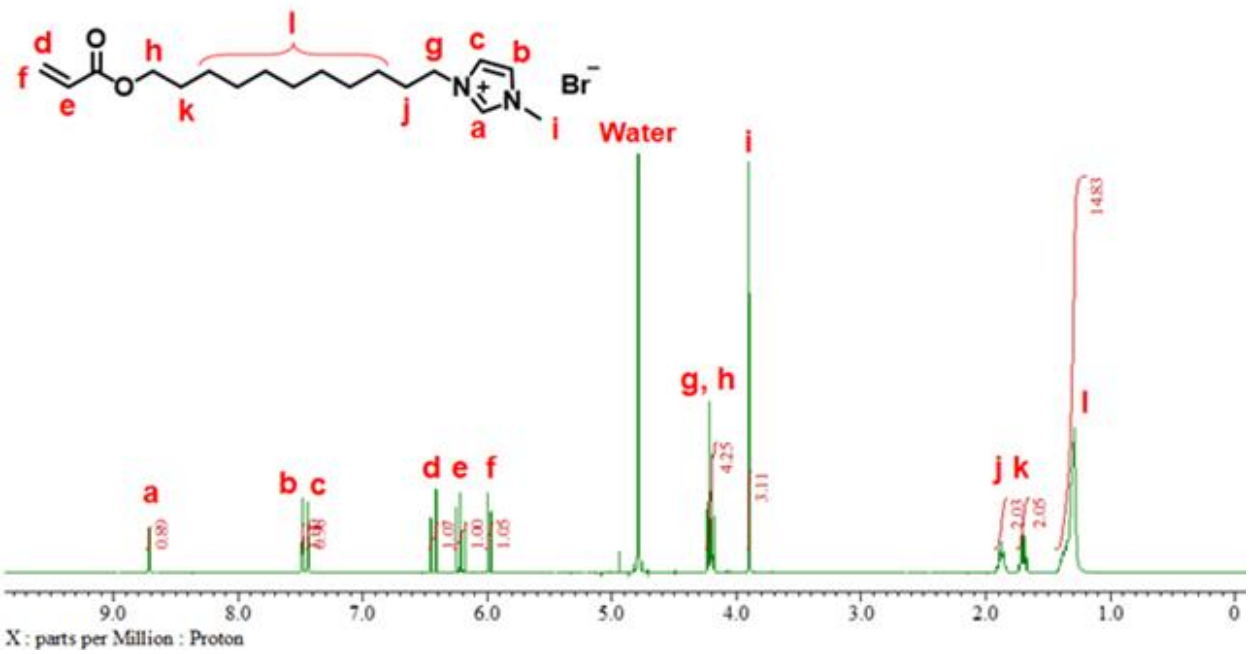

Figure S1. 400 MHz ^{1}H NMR spectrum of ImC11 in D_2O at 25 °C.

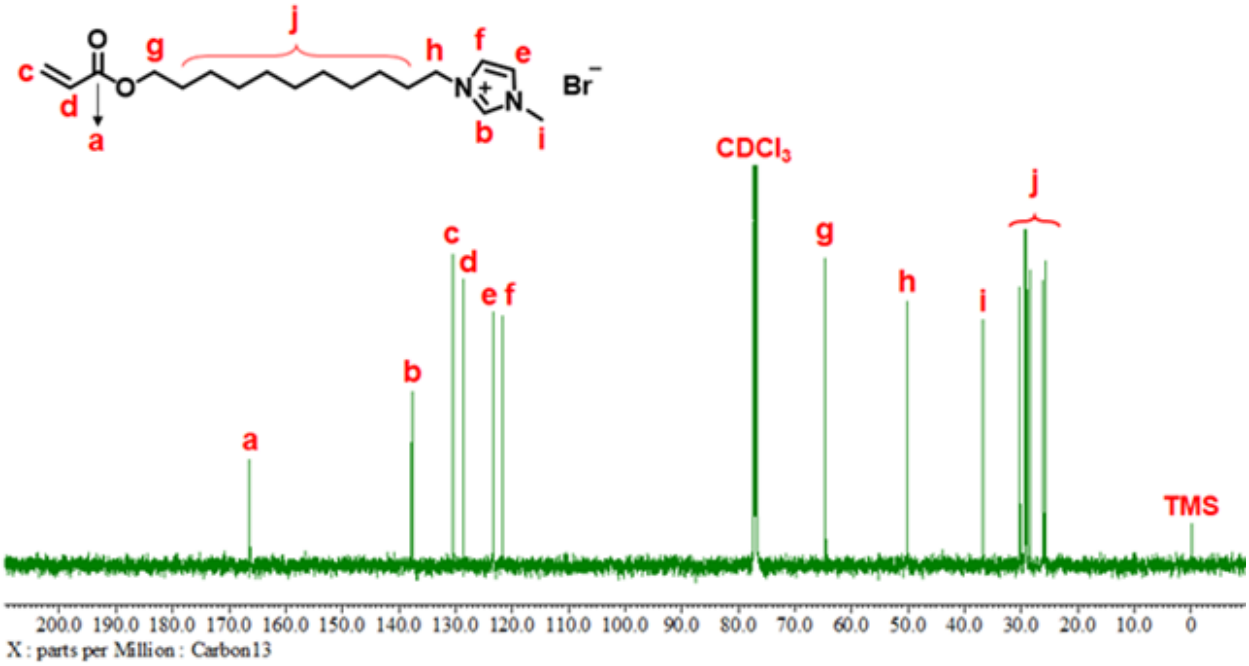

Figure S2. 125 MHz ^{13}C NMR spectrum of ImC11 in $CDCl_3$ at 25 °C.

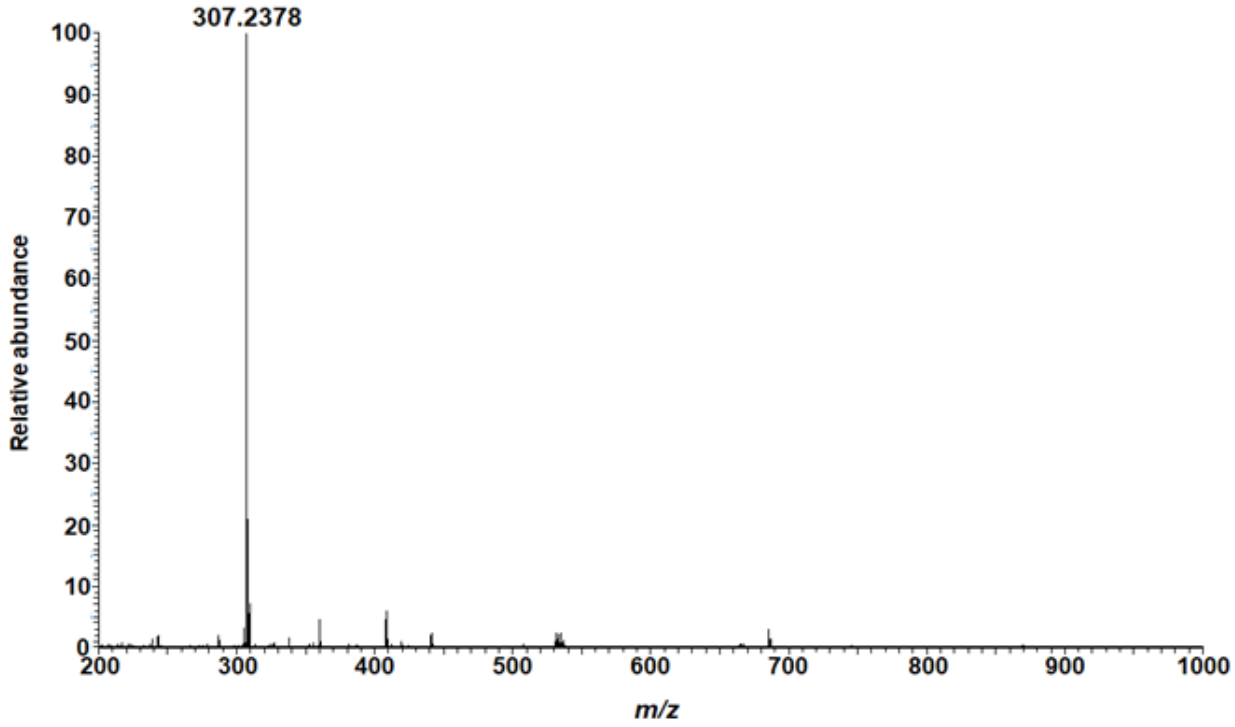

Figure S3. ESI mass spectrum of ImC11.

Preparation of 1-(11-acryloyloxyundecyl)-pyridinium bromide (PyC11)

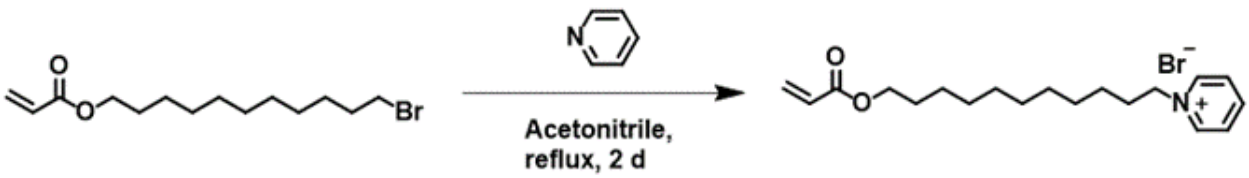

Scheme S2. Preparation of PyC11.

4-(11-Acryloyloxyundecyl)-4'-bipyridinium bromide (3.05 g, 10 mmol) and pyridine (1.58 g, 20 mmol) were dissolved in acetonitrile (20 mL), and the solution was refluxed for 2 days. The resulting solution was poured into diethyl ether to precipitate the crude product, which was filtrated and washed with diethyl ether. PyC11 was obtained as white solid (2.75 g, 72% yield).

^{1}H NMR (400 MHz, D_2O): δ = 8.86 (dd, J = 6.4, 1.2 Hz, 2H), 8.56 (dd, J = 8.0, 1.2 Hz, 1H), 8.08 (t, J = 7.2 Hz, 2H), 6.43 (dd, J = 17.2, 1.2 Hz, 1H), 6.22 (dd, J = 17.2, 10.4 Hz, 1H), 5.98 (dd, J = 10.4, 1.2 Hz, 1H), 4.62 (t, J = 7.2 Hz, 2H), 4.21 (t, J = 6.8 Hz, 2H), 2.03 (quin, J = 7.2 Hz, 2H), 1.70 (quin, J = 6.8 Hz, 2H), 1.42–1.28 (m, 14H) (see **Figure S4**).

^{13}C NMR (125 MHz, $CDCl_3$): δ = 166.32, 145.08, 130.42, 128.58, 128.39, 64.61, 62.12, 31.93, 29.30, 29.28, 29.20, 29.08, 28.95, 28.51, 25.98, 25.79 (see **Figure S5**).

ESI-LIT-orbitrap MS: *m*/*z*

Calcd. for $C_{19}H_{30}NO_2$ ([M - Br]$^+$): 304.2271;

Found: 304.2269 (see **Figure S6**)

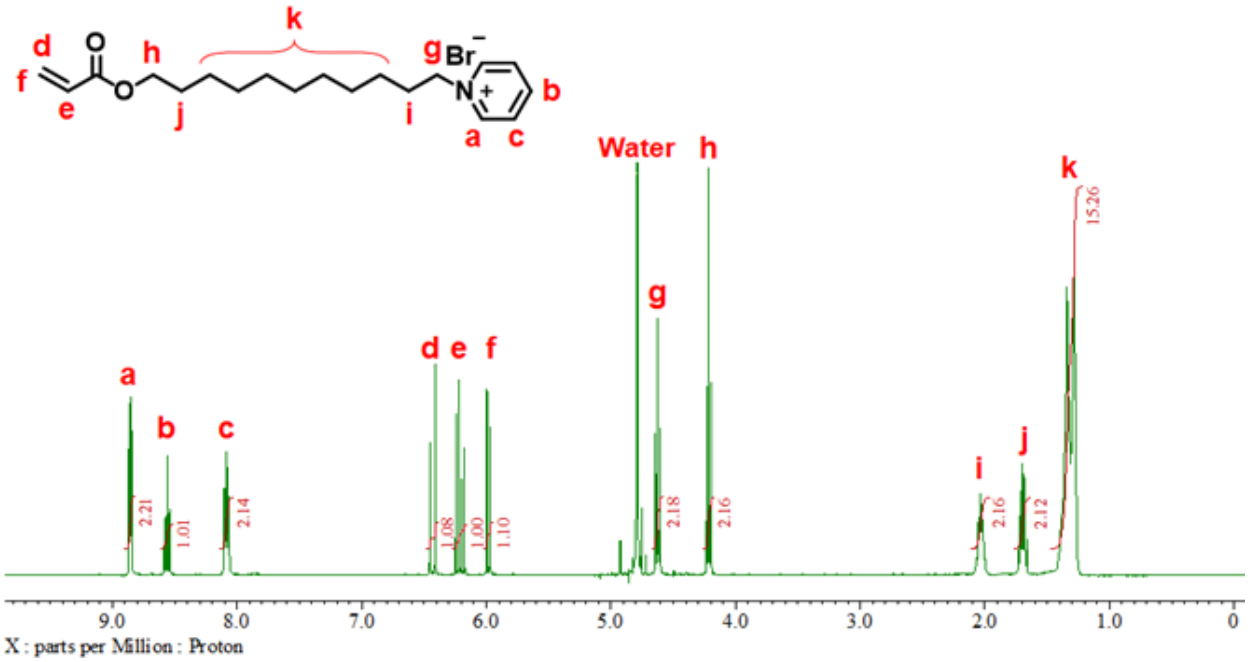

Figure S4. 400 MHz ^{1}H NMR spectrum of PyC11 in D_2O at 25 °C.

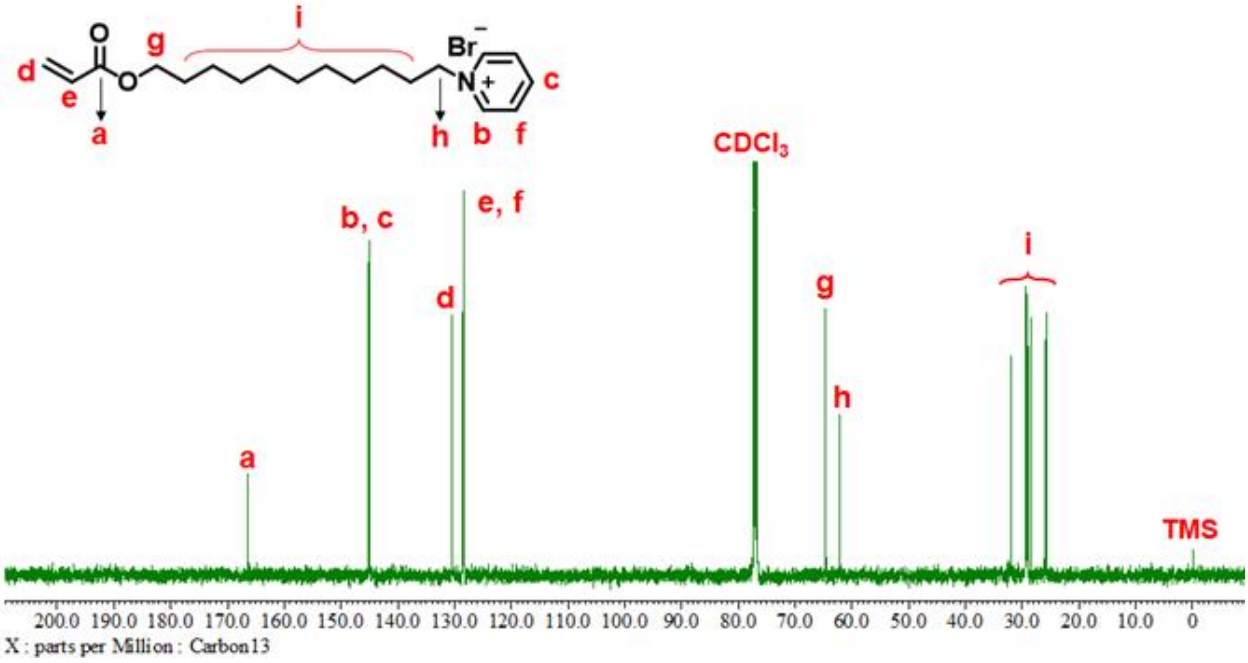

Figure S5. 125 MHz ^{13}C NMR spectrum of PyC11 in $CDCl_3$ at 25 °C.

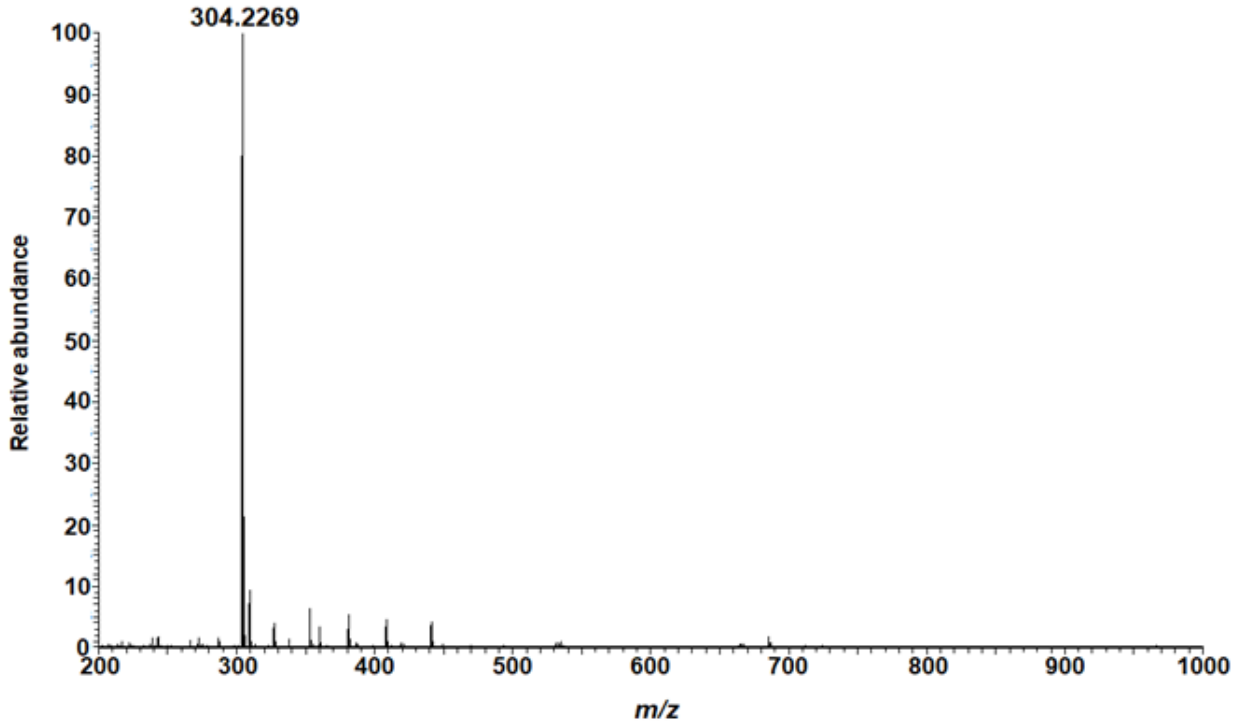

Figure S6. ESI mass spectrum of PyC11.

Preparation of 11-Acryloyloxyundecyl trimethylammonium bromide (TMAmC11)

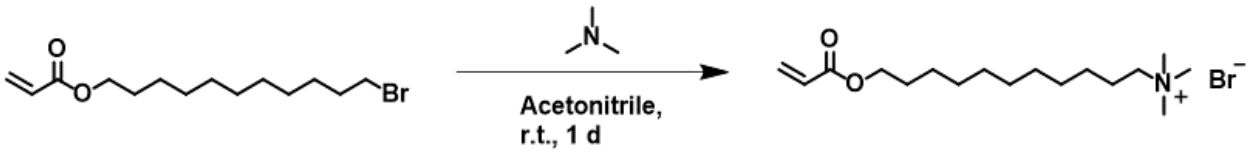

Scheme S3. Preparation of TMAmC11.

Trimethylamine in acetonitrile (2.0 M, 10 mL, 20 mmol) was added to a solution of 4-(11-acryloyloxyundecyl)-4'-bipyridinium bromide (2.02 g, 6.6 mmol) in acetonitrile (10 mL), and the solution was stirred at r.t. for 1 day. After the resulting solution was evaporated, the residue was dissolved in methanol and poured into diethyl ether to precipitate the product. TMAmC11 was separated from the mixture by centrifugation and obtained as white solid (2.16 g, 89% yield).

^{1}H NMR (400 MHz, D_2O): δ = 6.43 (dd, J = 17.2, 1.2 Hz, 1H), 6.22 (dd, J = 17.2, 10.8 Hz, 1H), 5.99 (dd, J = 10.8, 1.2 Hz, 1H), 4.22 (t, J = 6.8 Hz, 2H), 3.32 (m, 2H), 3.12 (s, 9H), 1.80 (quin, J = 6.4 Hz, 2H), 1.71 (quin, J = 6.8 Hz, 2H), 1.41–1.32 (m, 14H) (see **Figure S7**).

^{13}C NMR (125 MHz, $CDCl_3$): δ = 166.31, 130.42, 128.58, 66.97, 64.60, 53.34, 29.30, 29.24, 29.22, 29.11, 29.08, 28.51, 26.09, 25.80, 23.13 (see **Figure S8**).

ESI-LIT-orbitrap MS: *m*/*z*

Calcd. for $C_{17}H_{34}NO_2$ ($[M - Br]^+$): 284.2584;

Found: 284.2444 (see **Figure S9**)

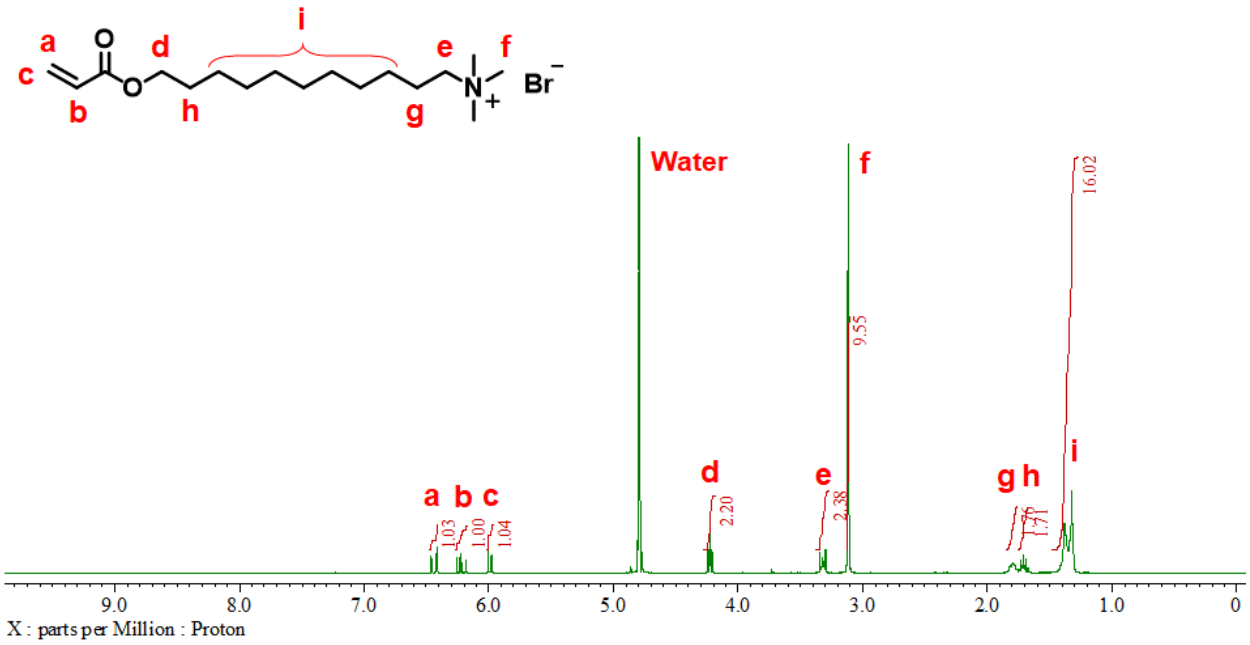

Figure S7. 400 MHz ^{1}H NMR spectrum of TMAmC11 in D_2O at 25 °C.

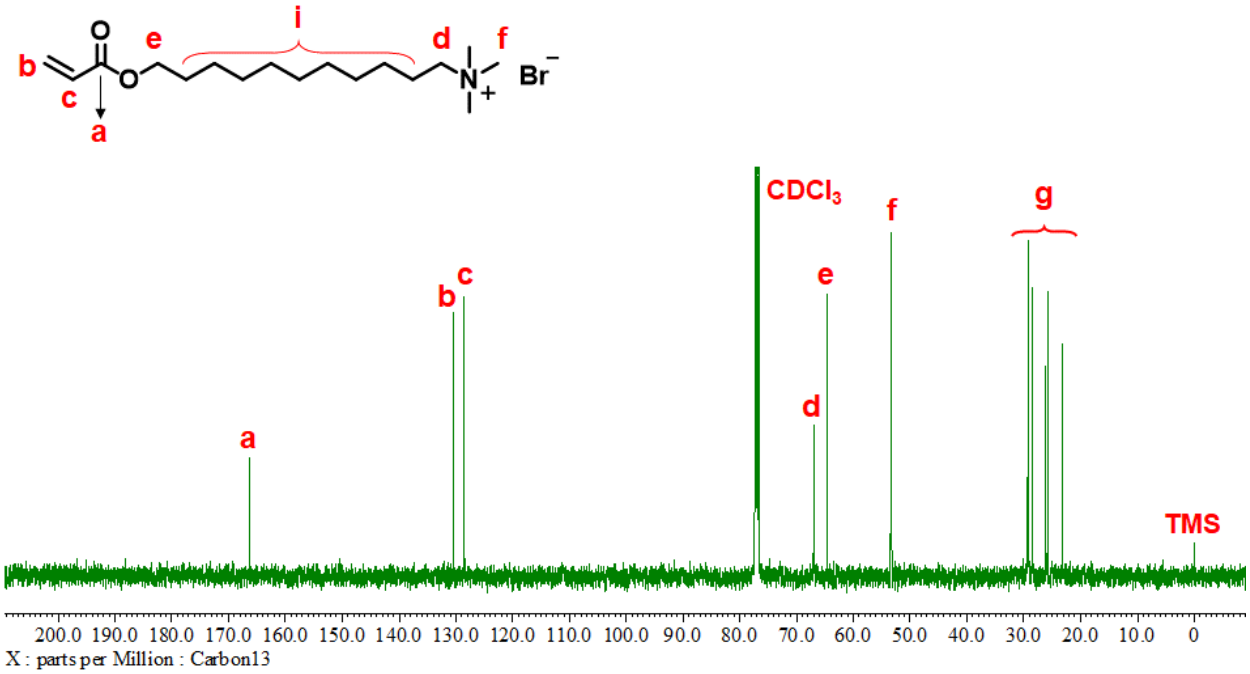

Figure S8. 125 MHz ^{13}C NMR spectrum of TMAmC11 in $CDCl_3$ at 25 °C.

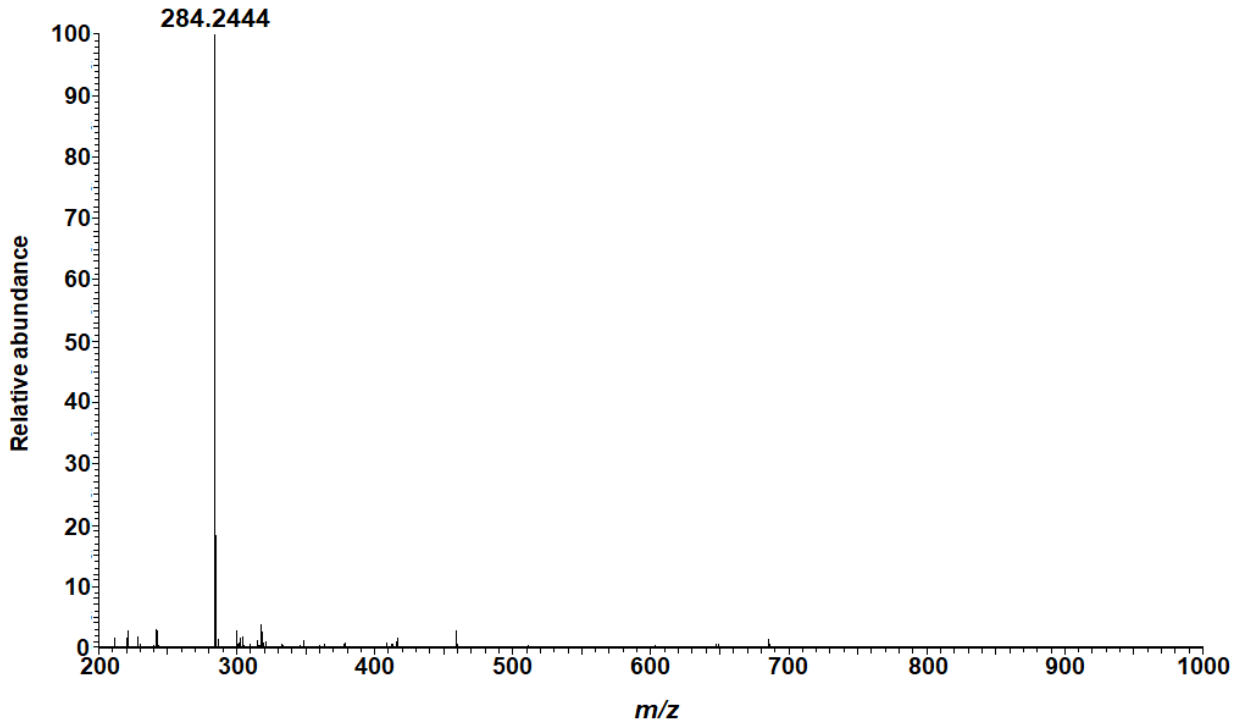

Figure S9. ESI mass spectrum of TMAmC11.

3. Formation of the inclusion complexes of αCDAAmMe with guest monomers

3-1. Formation of the inclusion complexes of αCDAAmMe with ImC11

Figures S10–11 shows the 2D ROESY NMR spectrum of the mixture of αCD with ImC11 in D_2O. Correlations were observed between the inner protons ($C^{3,5,6}H$) of the αCD residues and the protons of the alkyl chain of ImC11, indicating that the alkyl group of ImC11 is included in the αCDAAmMe.

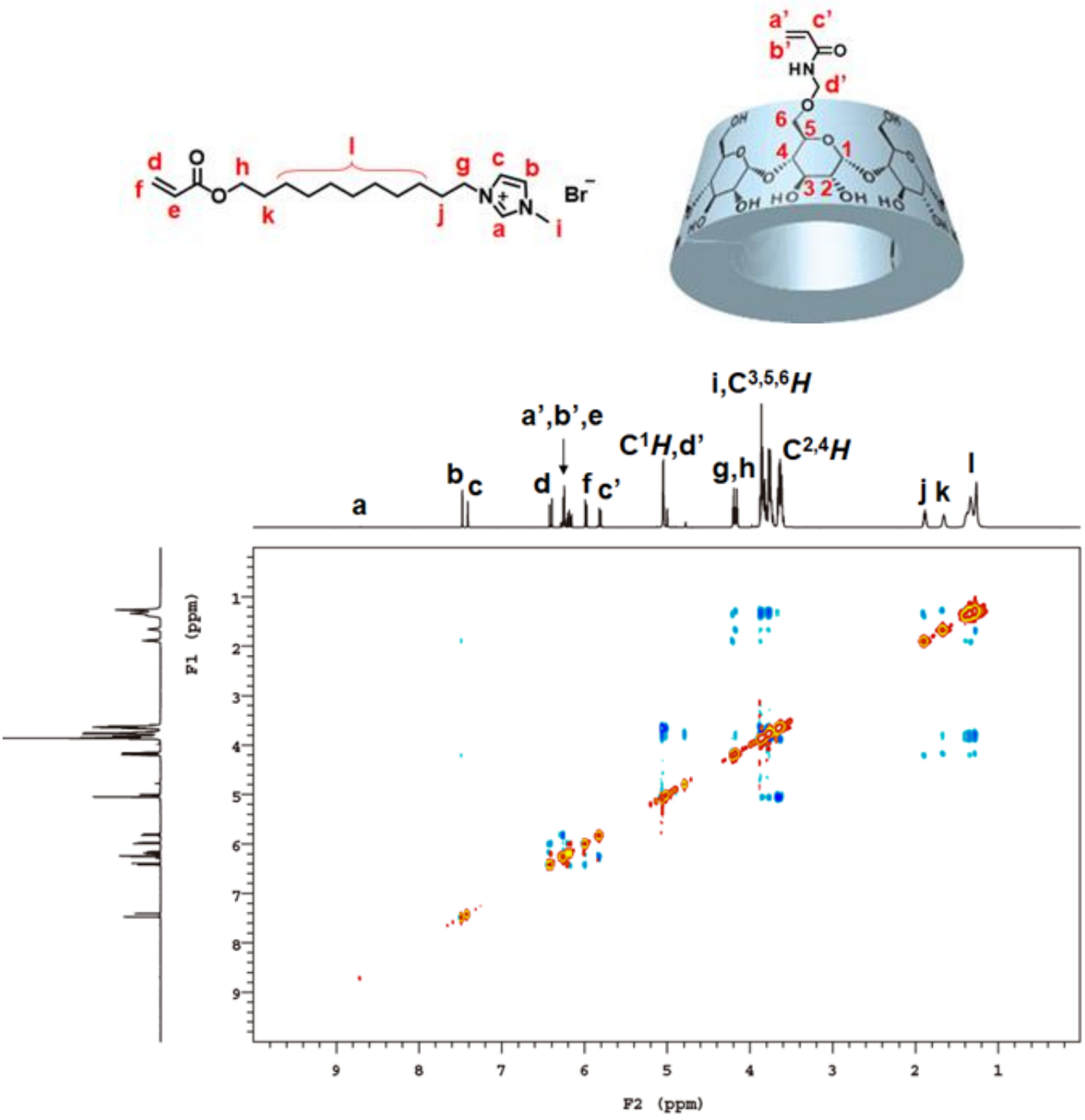

Figure S10. 600 MHz 2D ROESY NMR spectrum of a mixture of αCDAAmMe (10 mM) and ImC11 (10 mM) in D_2O at 30 °C.

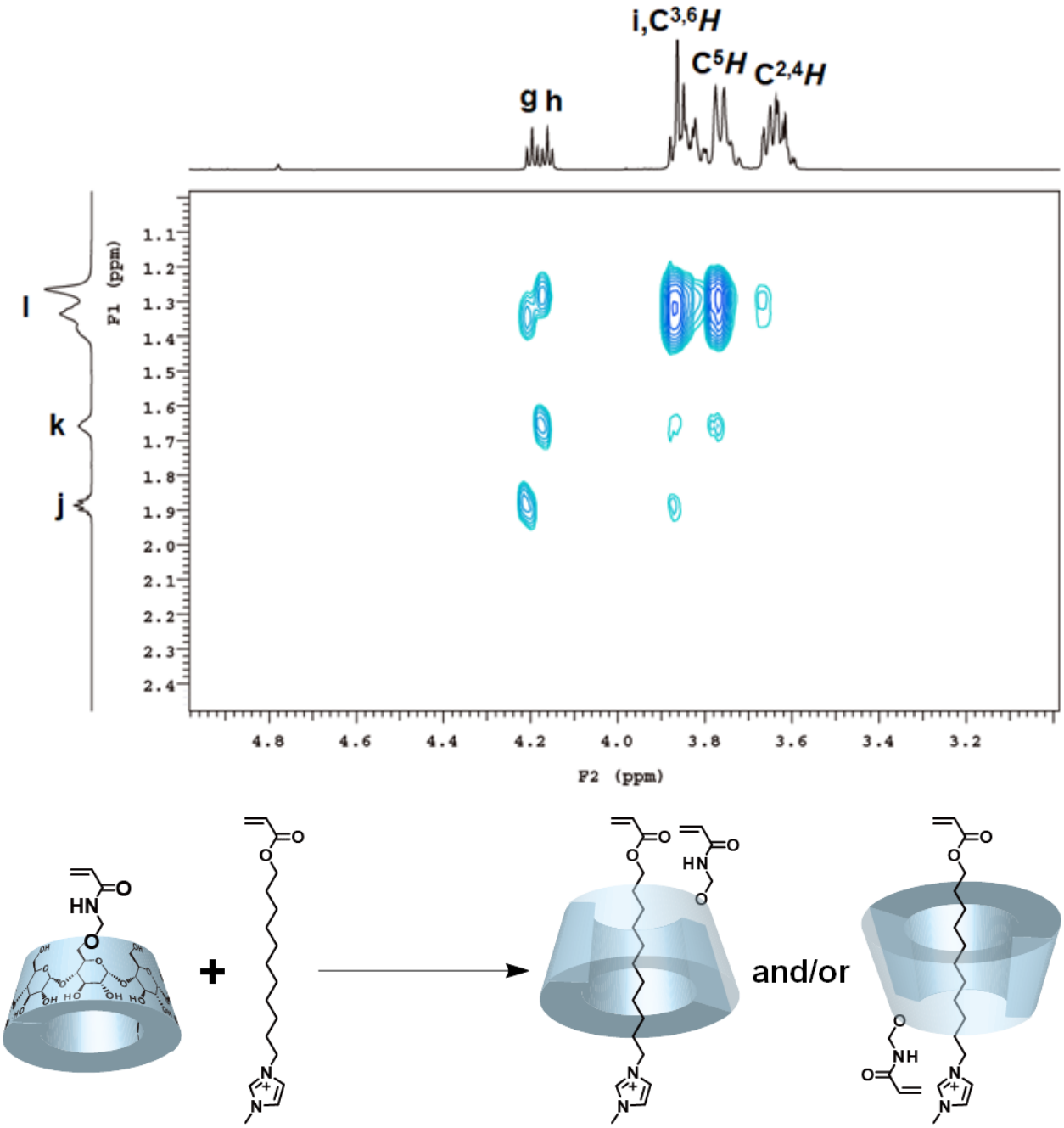

Figure S11. Zoomed view of Fig. S10 and the proposed structure of the inclusion complex.

3-2. Formation of the inclusion complexes of αCDAAmMe with Py11

Figures S12–13 shows the 2D ROESY NMR spectrum of the mixture of αCDAAmMe with PyC11 in D_2O. Correlations were observed between the inner protons ($C^{3,5,6}H$) of the αCDAAmMe residues and the protons of the alkyl chain of PyC11, indicating that the alkyl group of PyC11 is included in the αCDAAmMe.

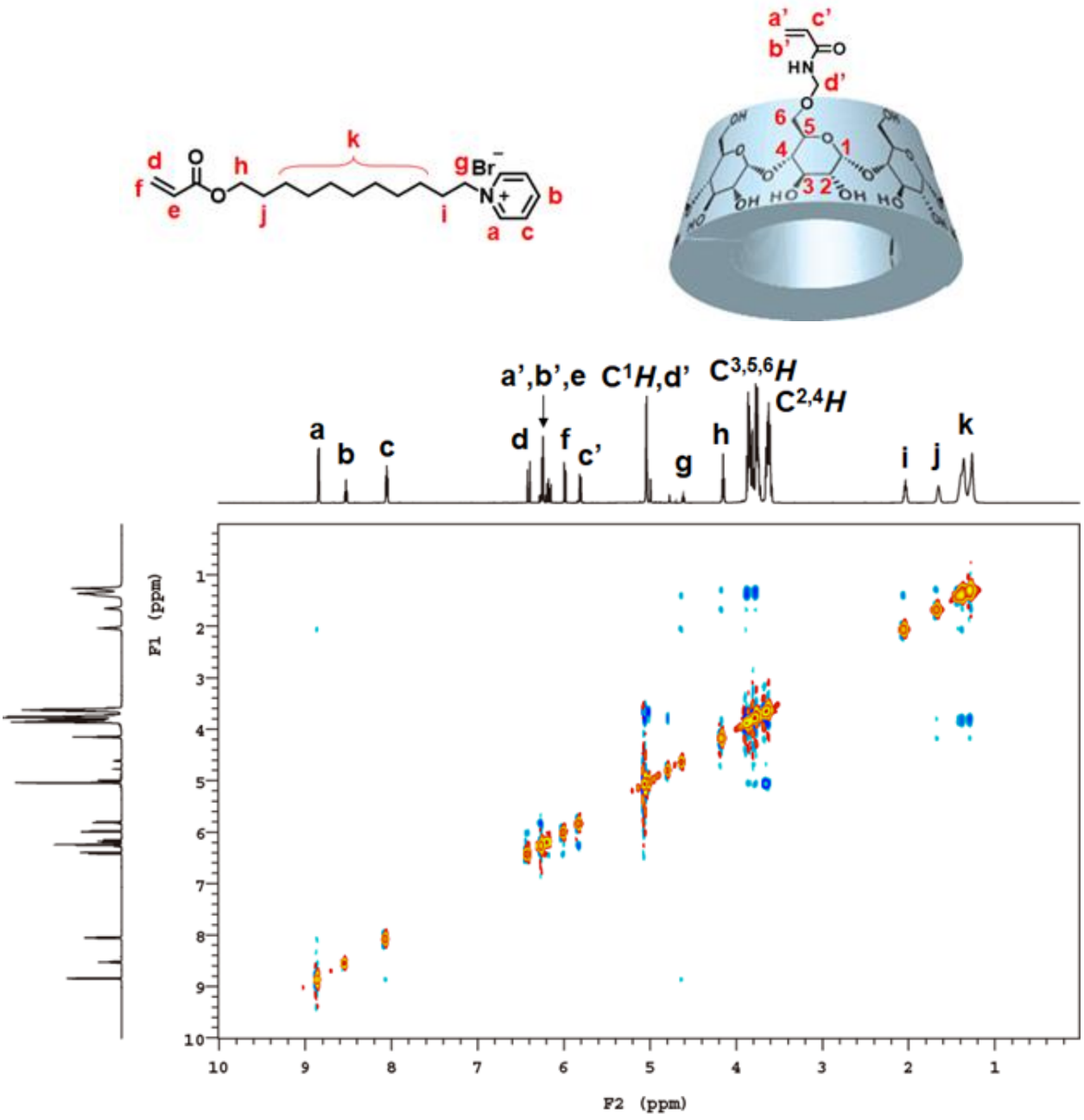

Figure S12. 600 MHz 2D ROESY NMR spectrum of a mixture of αCDAAmMe (10 mM) and PyC11 (10 mM) in D_2O at 30 °C.

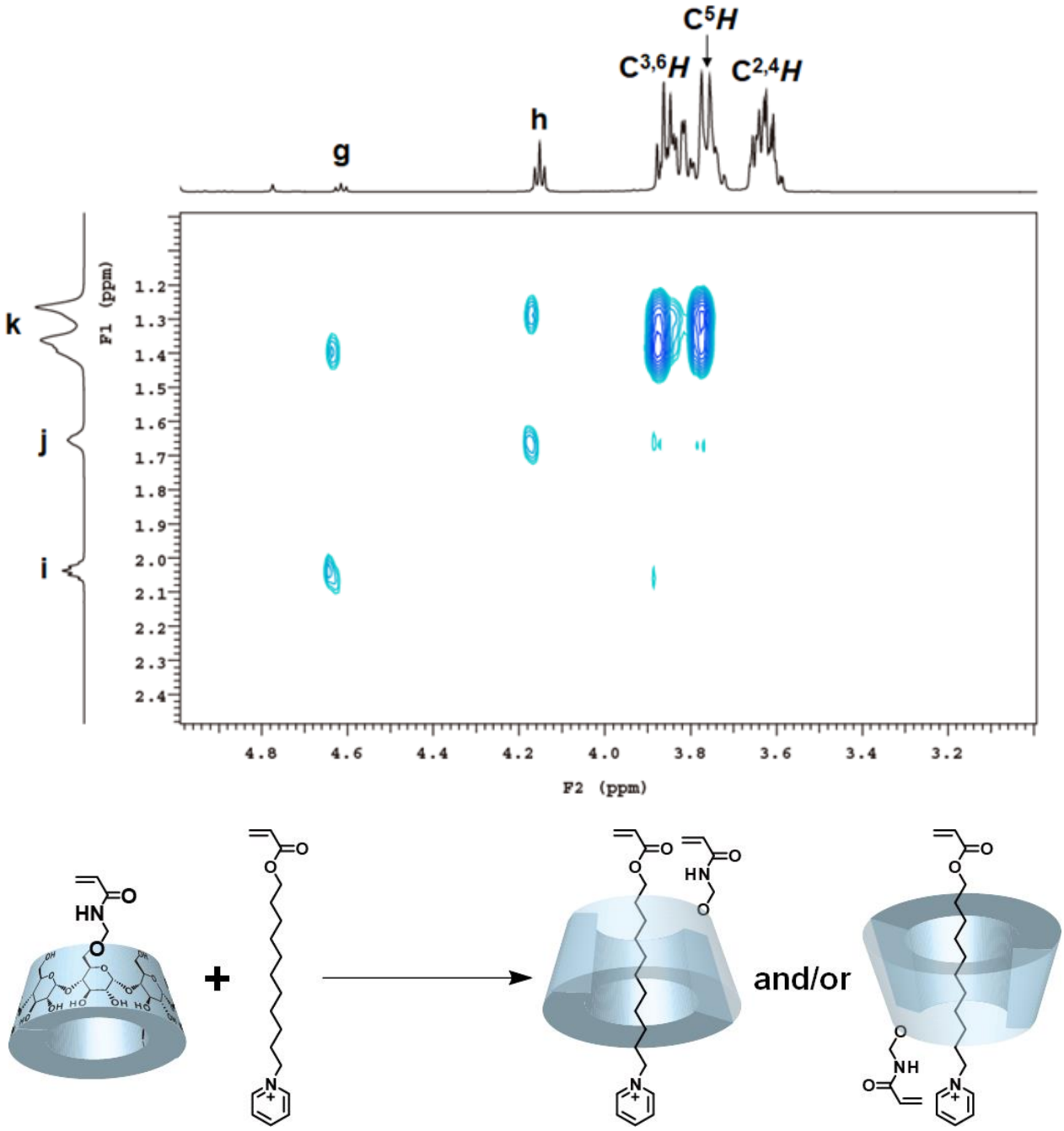

Figure S13. Zoomed view of Fig, S12 and the proposed structure of the inclusion complex.

3-3. Formation of the inclusion complexes of αCDAAmMe with TMAm11

Figures S14–15 shows the 2D ROESY NMR spectrum of the mixture of αCDAAmMe with TMAmC11 in D_2O. Correlations were observed between the inner protons ($C^{3,5,6}H$) of the αCDAAmMe residues and the protons of the alkyl chain of TMAmC11, indicating that the alkyl group of TMAmC11 is included in the αCDAAmMe.

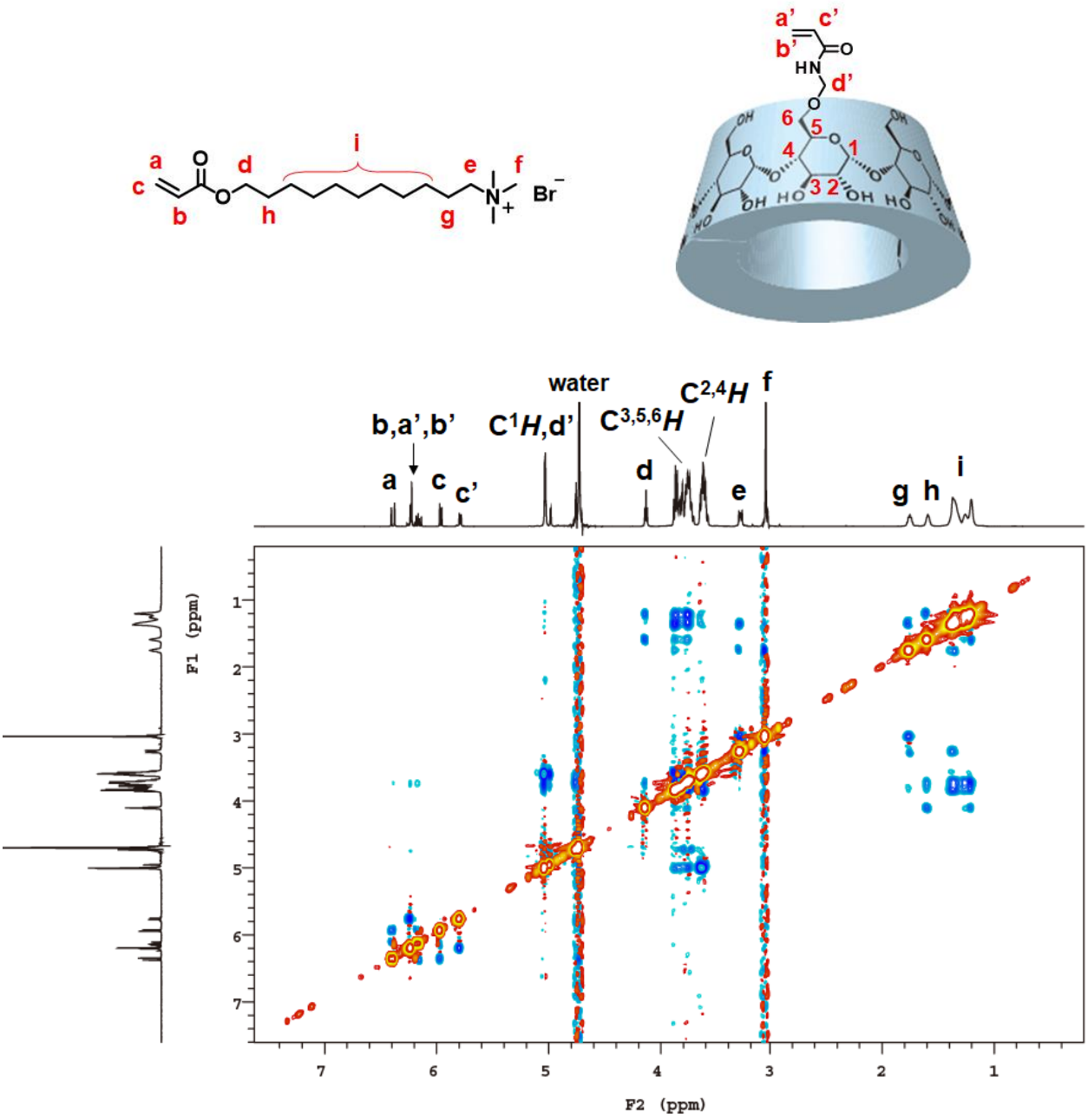

Figure S14. 600 MHz 2D ROESY NMR spectrum of a mixture of αCDAAmMe (10 mM) and TMAmC11 (10 mM) in D_2O at 30 °C.

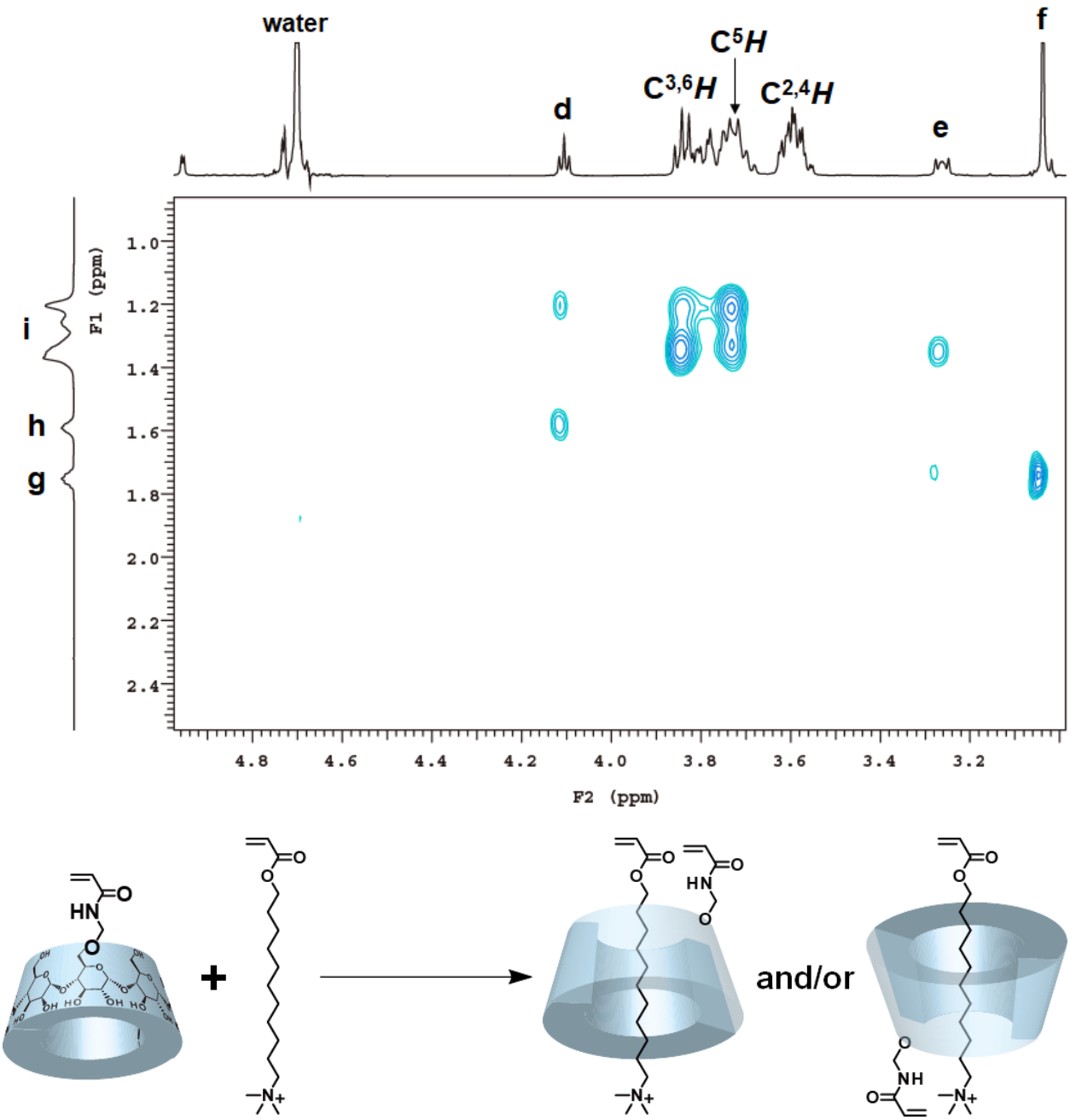

Figure S15. Zoomed view of Fig, S14 and the proposed structure of the inclusion complex.

4. Association constant of the inclusion complex of αCDAAmMe and guest monomers

We performed ^{1}H NMR measurements to estimate the association constant (K_a) of 1:1 complexation between αCDAAmMe and guest monomers using nonlinear least-squares method. All chemical shifts were referenced to the residual solvent peaks of deuterated DMSO as external standards (δ = 2.49 ppm). We plotted $\Delta\delta_{obs}$ as a function of $[H]_0/[[G]_0$. Fitting equation as shown below was used to determine K_a.

$$\Delta\delta_{obs} = \frac{\Delta\delta_{max}}{2K_a[G]_0}\left[1 + K_a[H]_0 + K_a[G]_0 - \left\{(1 + K_a[H]_0 + K_a[G]_0)^2 - 4K_a{}^2[H]_0[G]_0\right\}^{1/2}\right] \quad (1)$$

$\Delta\delta_{obs}$: Observed change in chemical shift

$\Delta\delta_{max}$: Maximum change in chemical shift (fitting parameter)

K_a: Association constant (fitting parameter)

$[H]_0$: Concentration of host

$[G]_0$: Concentration of guest (fixed parameter)

K_a of αCDAAmMe with C12 could not be estimated due to hydrophobicity of C12 and the inclusion complex. Therefore, we referred to K_a of αCD with *n*-dodecyl(ester)-acrylamide polymer (1200 M^{-1})[3].

K_a of αCDAAmMe with VC11 was calculated as 3.5×10^3 M^{-1} in our previous work.[4]

We cited K_a of αCD with N^1,N^1,N^1,N^{10},N^{10},N^{10}-hexamethyldecane-1,10-diaminium (1540 M^{-1})[5] as a model of αCDAAmMe with TMAmC11.

4-1. Association constant of the inclusion complex of αCDAAmMe and ImC11

Figure S16 shows ^{1}H NMR spectra of a mixture of ImC11 (1.0 mM) and αCDAAmMe (0, 0.5, 1.0, 1.5, 2.5, 3.5, 5.0, or 7.5 mM) in D_2O. Chemical shift values of b, f, and l protons of ImC11 were analyzed to obtain K_a (**Figures S17 and S18**). Note that waveform separation analysis of l proton (**Figure S18a**) was carried out by non-linear least square curve fitting method to determine precise position of peak top (Equation (2) was used for curve fitting). K_a for ImC11 and αCDAAmMe was calculated as $(1.7 \pm 0.35) \times 10^3$ M^{-1}.

$$I = \sum_{i=1}^{n} \left\{ \frac{A_i}{\sqrt{2\pi {\sigma_i}^2}} \exp\left(-\frac{\delta - \delta_i}{2{\sigma_i}^2} \right) \right\} + a\delta + b \qquad (2)$$

I (signal intensity) is a function of δ (chemical shift), where A_i, σ_i, δ_i, a, and b are fitting parameters. Number of signals (n) was 3.

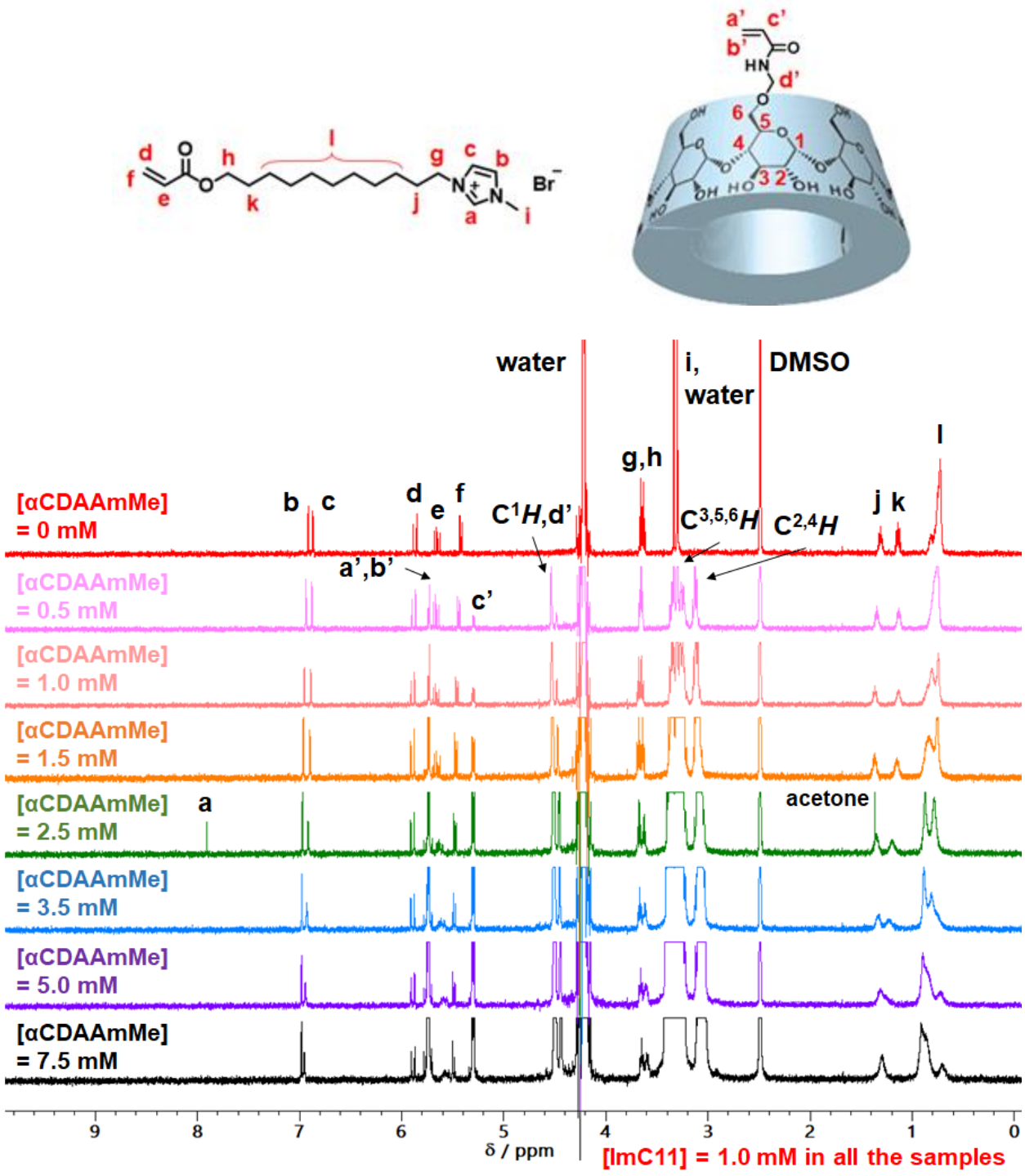

Figure S16. 500 MHz ^{1}H NMR spectra of a mixture of ImC11 (1.0 mM) and αCDAAmMe (0, 0.5, 1.0, 1.5, 2.5, 3.5, 5.0, or 7.5 mM) in D_2O at 25 °C.

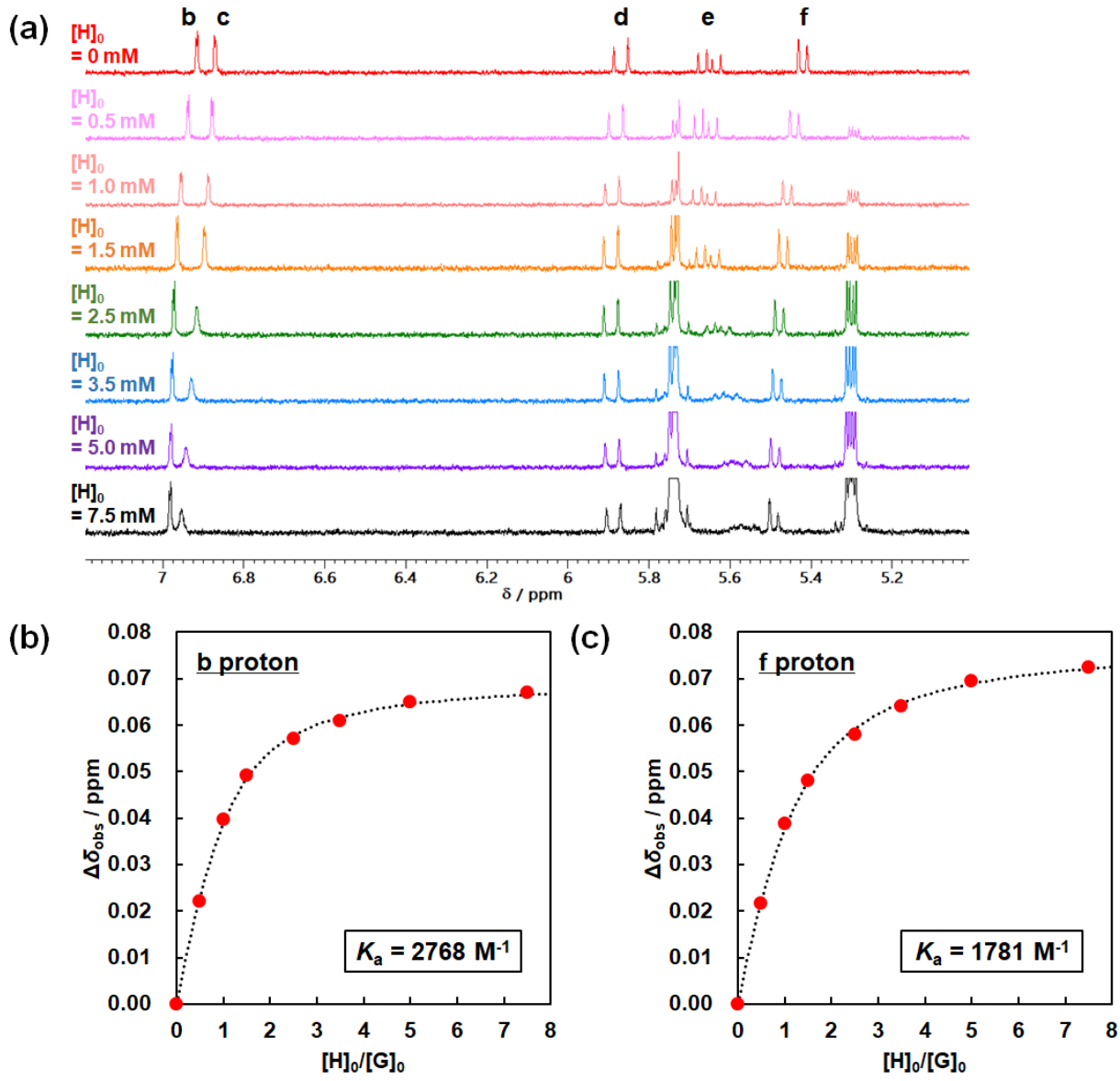

Figure S17. (a) Partial spectra of ImC11 with αCDAAmMe at δ in the range of 5.0 to 7.2 ppm. **(b)**, **(c)** Results of non-linear least squares fitting (dot lines) for plot of the chemical shift values of ImC11 and the molar ratio $[H]_0/[[G]_0$ (red filled circles). Association constants of the 1:1 complexation between αCDAAmMe and ImC11 were determined by the fitting as 2768 M^{-1} and 1781 M^{-1}.

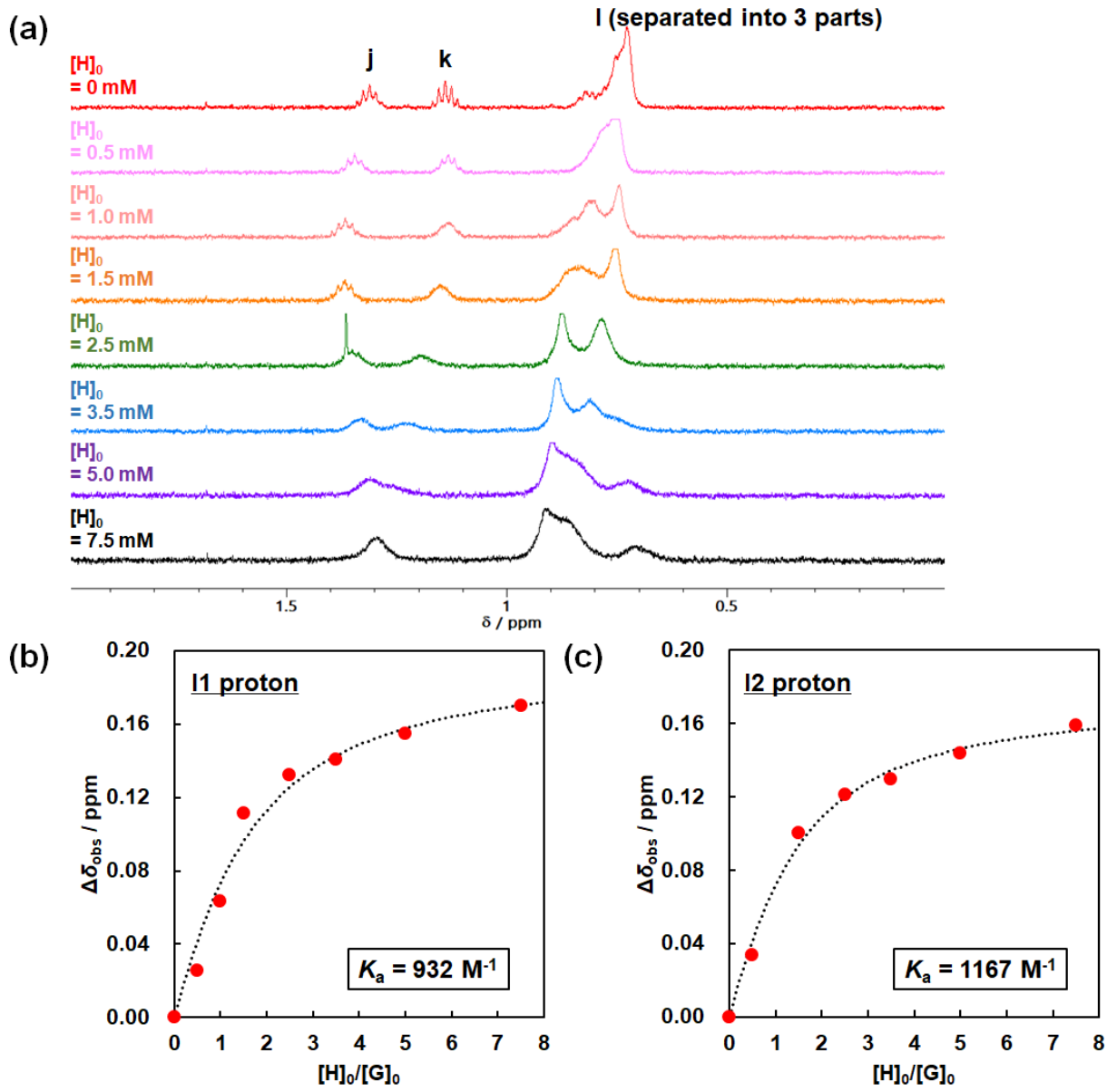

Figure S18. (a) Partial spectra of ImC11 with αCDAAmMe at δ in the range of 0 to 2.0 ppm. **(b)**, **(c)** Results of non-linear least squares fitting (dot lines) for plot of the chemical shift value of ImC11 and the molar ratio $[H]_0/[[G]_0$ (red filled circles). Association constants of the 1:1 complexation between αCDAAmMe and ImC11 were determined by the fitting as 932 M^{-1} and 1167 M^{-1}.

4-2. Association constant of the inclusion complex of αCDAAmMe and PyC11

Figure S19 shows ^{1}H NMR spectra of a mixture of PyC11 (1.0 mM) and αCDAAmMe (0, 0.5, 1.0, 1.5, 2.5, 3.5, 5.0, or 7.5 mM) in D_2O. Chemical shift values of a, f, and k protons of PyC11 were analyzed to obtain K_a (**Figures S20 and S21**). Note that waveform separation analysis of k proton was carried out by non-linear least square curve fitting method to determine precise position of peak top (Equation (2) was used for curve fitting. Number of signals (n) was 4). K_a for PyC11 and αCDAAmMe was calculated as $(1.7 \pm 0.51) \times 10^3$ M^{-1}.

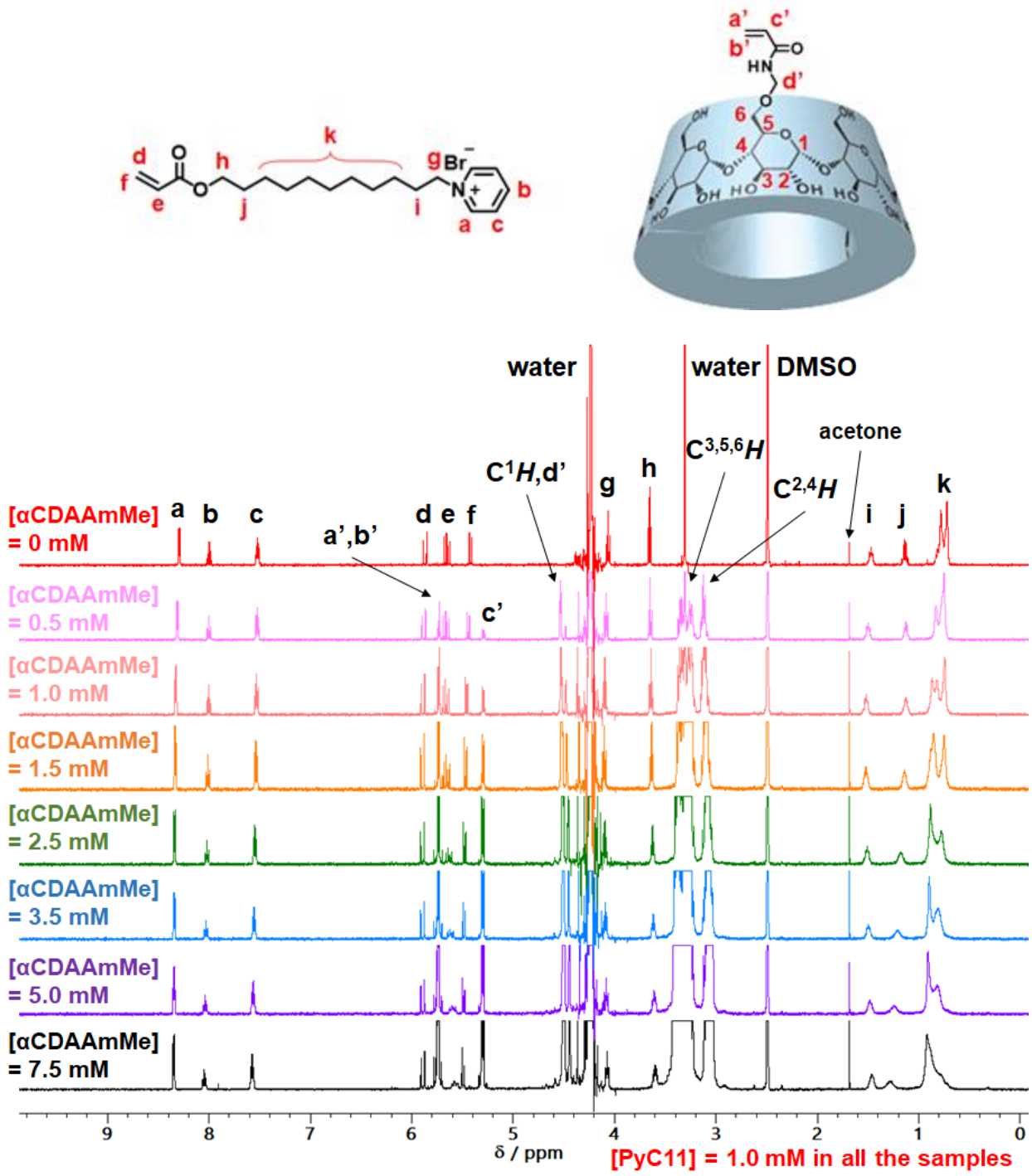

Figure S19. 500 MHz ^{1}H NMR spectra of a mixture of PyC11 (1.0 mM) and αCDAAmMe (0, 0.5, 1.0, 1.5, 2.5, 3.5, 5.0, or 7.5 mM) in D_2O at 25 °C.

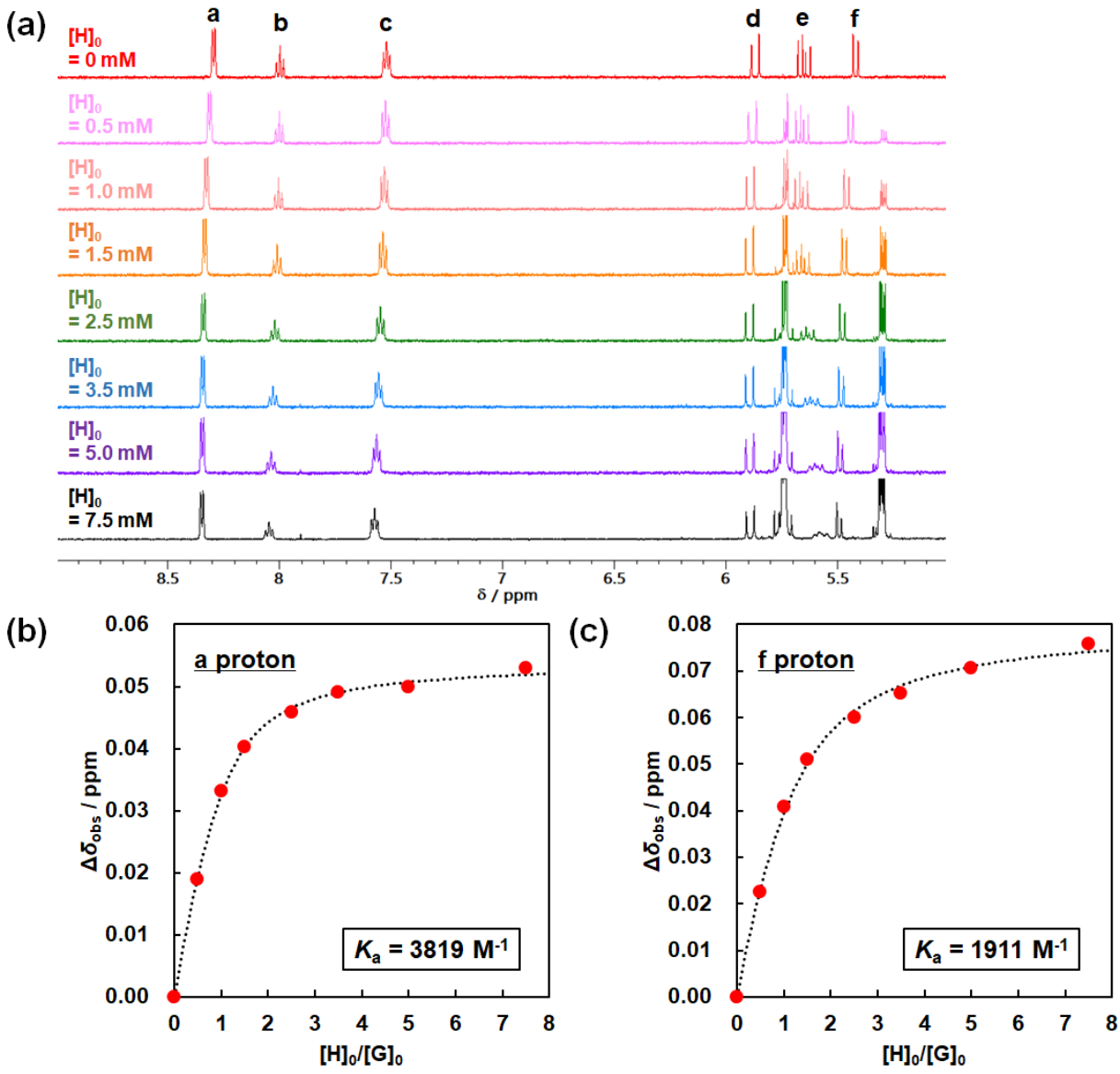

Figure S20. (a) Partial spectra of PyC11 with αCDAAmMe at δ in the range of 5.0 to 9.0 ppm. **(b)**, **(c)** Results of non-linear least squares fitting (dot lines) for plot of the chemical shift values of PyC11 and the molar ratio $[H]_0/[[G]_0$ (red filled circles). Association constants of the 1:1 complexation between αCDAAmMe and PyC11 were determined by the fitting as 3819 M^{-1} and 1911 M^{-1}.

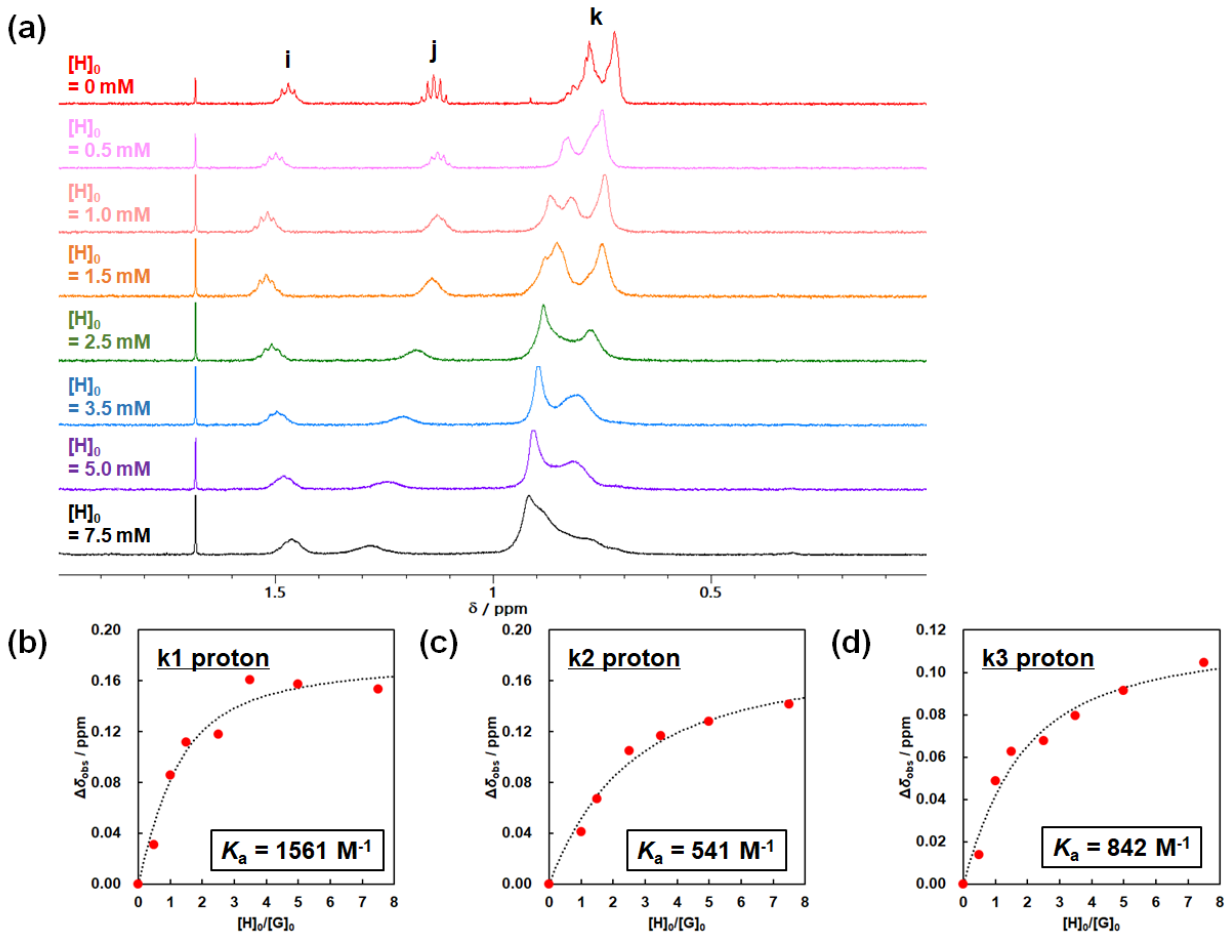

Figure S21. (a) Partial spectra of PyC11 with αCDAAmMe at δ in the range of 0 to 2.0 ppm. **(b)**, **(c)** and **(d)** Results of non-linear least squares fitting (dot lines) for plot of the chemical shift values of PyC11 and the molar ratio $[H]_0/[[G]_0$ (red filled circles). Association constants of the 1:1 complexation between αCDAAmMe and PyC11 were determined by the fitting as 1561 M^{-1}, 541 M^{-1} and 842 M^{-1}.

4-3. Relation between 1:1 complexation ratio and association constant

Figure S22 shows a theoretical curve depicting the K_a dependence of the complexation ratio calculated from concentrations of αCDAAmMe and guest monomers feed in pre-gel solution. Equation of the curve when $[H]_0$ and $[G]_0$ are 0.040 M is shown below. Concentrations of the inclusion complexes in pre-gel solutions were estimated at 0.035–0.037 mol/L.

$$Complexation\ ratio\ (\%) = \frac{50\left(25 + 2K_a - 5\sqrt{25 + 4K_a}\right)}{K_a} \quad (3)$$

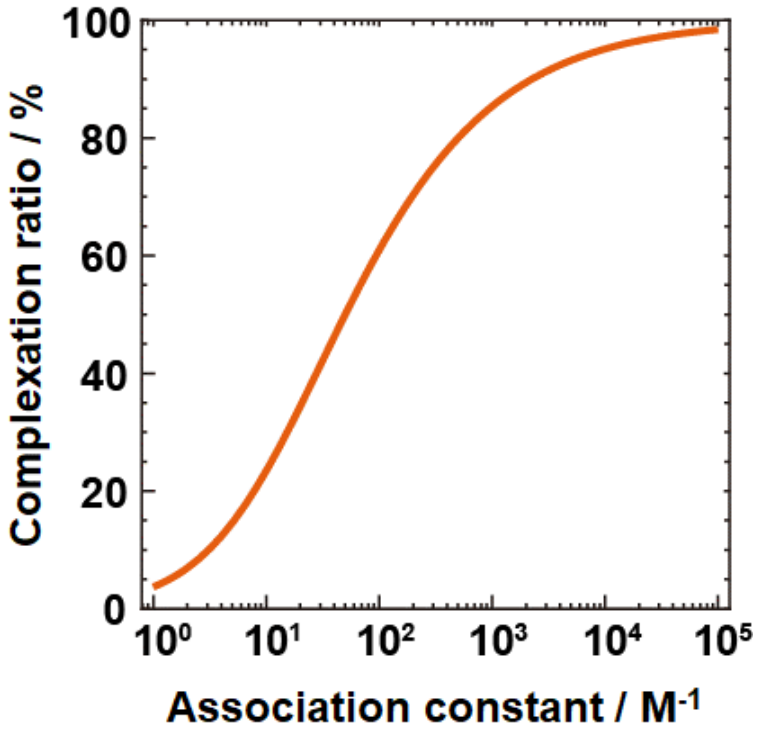

Figure S22. A theoretical curve depicting the K_a dependence of the 1:1 complexation ratio when $[H]_0$ and $[G]_0$ are 0.040 M.

5. Preparation of the supramolecular hydrogels

Preparation of the αCD-C12 hydrogel

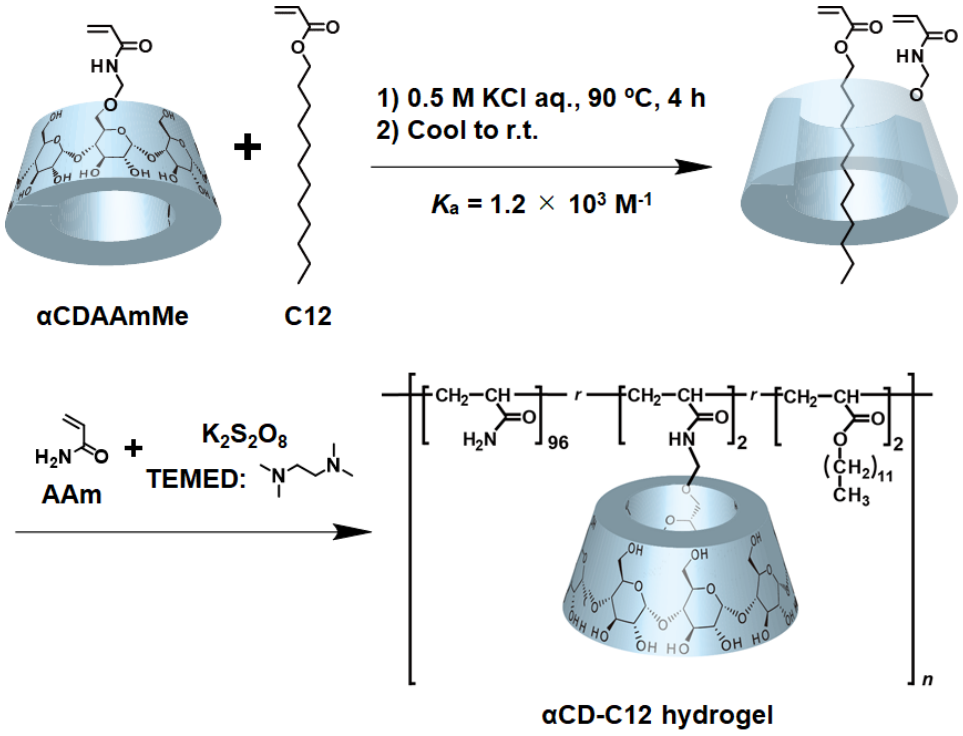

Scheme S4. Preparation of the αCD-C12 hydrogel.

αCDAAmMe (84 mg, 0.080 mmol) and dodecyl acrylate (C12; 19 mg, 0.080 mmol) were mixed in 0.5 M KCl aq. (2.0 mL) for 4 hours at 90 °C to form the host-guest inclusion complex. The inclusion complex of αCDAAmMe with C12 was copolymerized with acrylamide (AAm; the main chain monomer, 273 mg, 3.84 mmol) by using a redox initiator system (11 mg (0.040 mmol) of potassium persulfate ($K_2S_2O_4$) and 4.6 mg (0.040 mmol) of *N,N,N′,N′*-tetramethylethylenediamine (TEMED)) at room temperature. The solution gelated within 5 minutes to give a self-standing hydrogel. The hydrogel was characterized by FG-MAS NMR and IR spectroscopy (see below). The amounts of reagents and the solvent use are summarized in **Table S1**.

Preparation of the αCD-ImC11 hydrogel

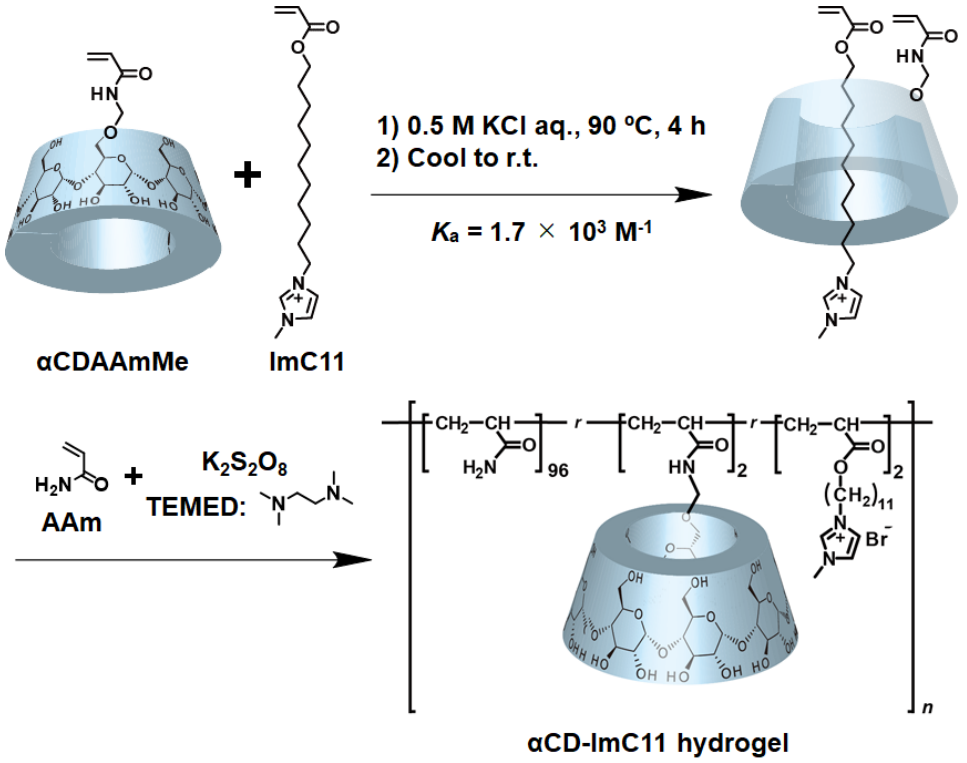

Scheme S5. Preparation of the αCD-ImC11 hydrogel.

αCDAAmMe (84 mg, 0.080 mmol) and ImC11 (31 mg, 0.080 mmol) were mixed in 0.5 M KCl aq. (2.0 mL) for 4 hours at 90 °C to form the host-guest inclusion complex. The inclusion complex of αCDAAmMe with PyC11 was copolymerized with acrylamide (AAm; the main chain monomer, 273 mg, 3.84 mmol) by using a redox initiator system (11 mg (0.040 mmol) of potassium persulfate ($K_2S_2O_4$) and 4.6 mg (0.040 mmol) of *N,N,N′,N′*-tetramethylethylenediamine (TEMED)) at room temperature. The solution gelated within 5 minutes to give a self-standing hydrogel. The hydrogel was characterized by FG-MAS NMR and IR spectroscopy (see below). The amounts of reagents and the solvent use are summarized in **Table S2**.

Preparation of the αCD-PyC11 hydrogel

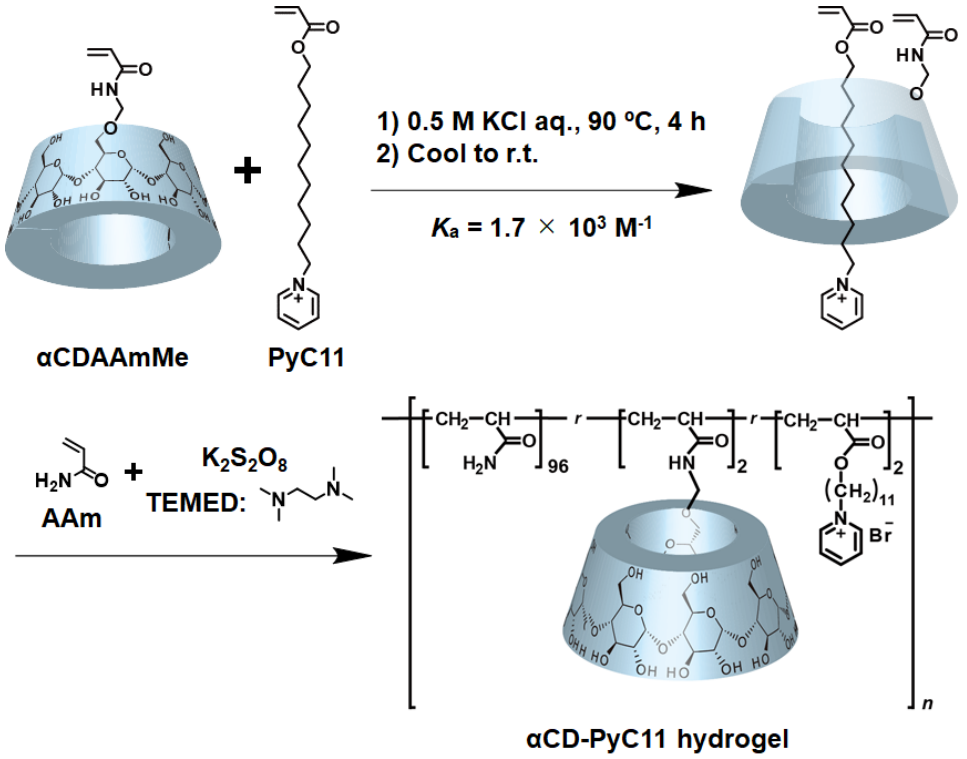

Scheme S6. Preparation of the αCD-PyC11 hydrogel.

αCDAAmMe (84 mg, 0.080 mmol) and PyC11 (31 mg, 0.080 mmol) were mixed in 0.5 M KCl aq. (2.0 mL) for 4 hours at 90 °C to form the host-guest inclusion complex. The inclusion complex of αCDAAmMe with PyC11 was copolymerized with acrylamide (AAm; the main chain monomer, 273 mg, 3.84 mmol) by using a redox initiator system (11 mg (0.040 mmol) of potassium persulfate ($K_2S_2O_4$) and 4.6 mg (0.040 mmol) of *N,N,N′,N′*-tetramethylethylenediamine (TEMED)) at room temperature. The solution gelated within 5 minutes to give a self-standing hydrogel. The hydrogel was characterized by FG-MAS NMR and IR spectroscopy (see below). The amounts of reagents and the solvent use are summarized in **Table S3**.

Preparation of the αCD-VC11 hydrogel

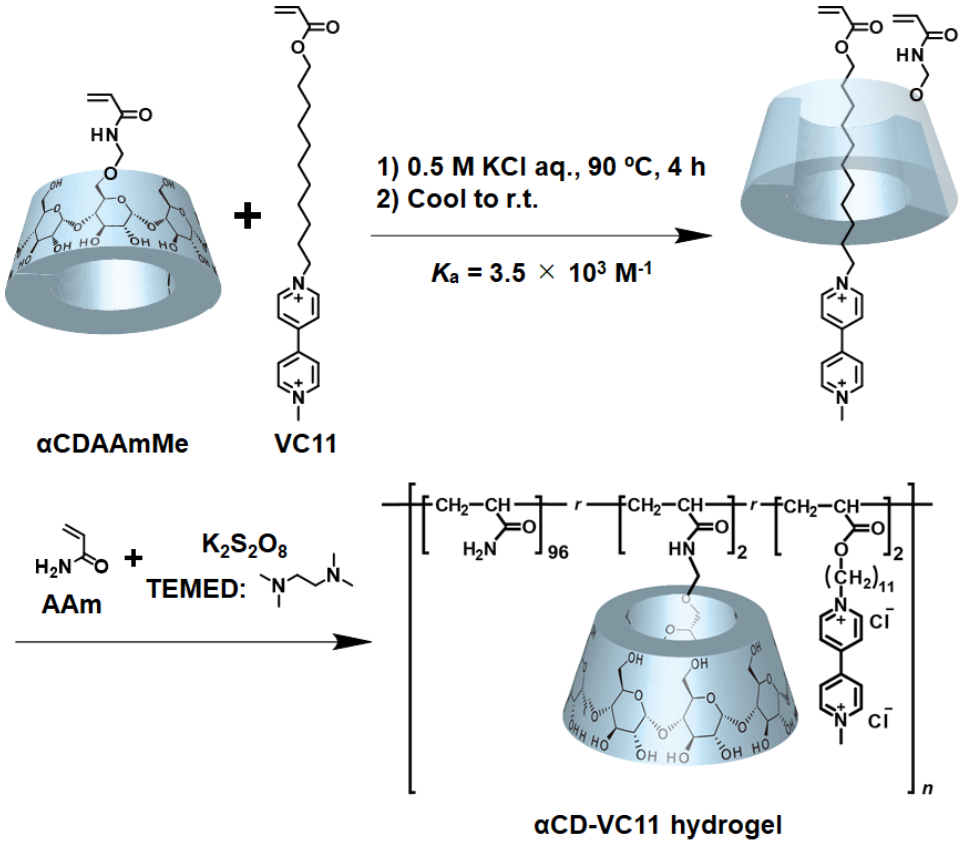

Scheme S7. Preparation of the αCD-VC11 hydrogel.

αCDAAmMe (84 mg, 0.080 mmol) and VC11 (37 mg, 0.080 mmol) were mixed in 0.5 M KCl aq. for 4 hours at 90 °C to form the host-guest inclusion complex. The inclusion complex of αCDAAmMe with VC11 was copolymerized with acrylamide (AAm; the main chain monomer, 273 mg, 3.84 mmol) by using a redox initiator system (11 mg (0.040 mmol) of potassium persulfate ($K_2S_2O_4$) and 4.6 mg (0.040 mmol) of *N,N,N′,N′*-tetramethylethylenediamine (TEMED)) at room temperature. The solution gelated within 5 minutes to give a self-standing hydrogel. The hydrogel were characterized by FG-MAS NMR and IR spectroscopy (see below). The amounts of reagents and the solvent use are summarized in **Table S4**.

Preparation of the αCD-TMAmC11 hydrogel

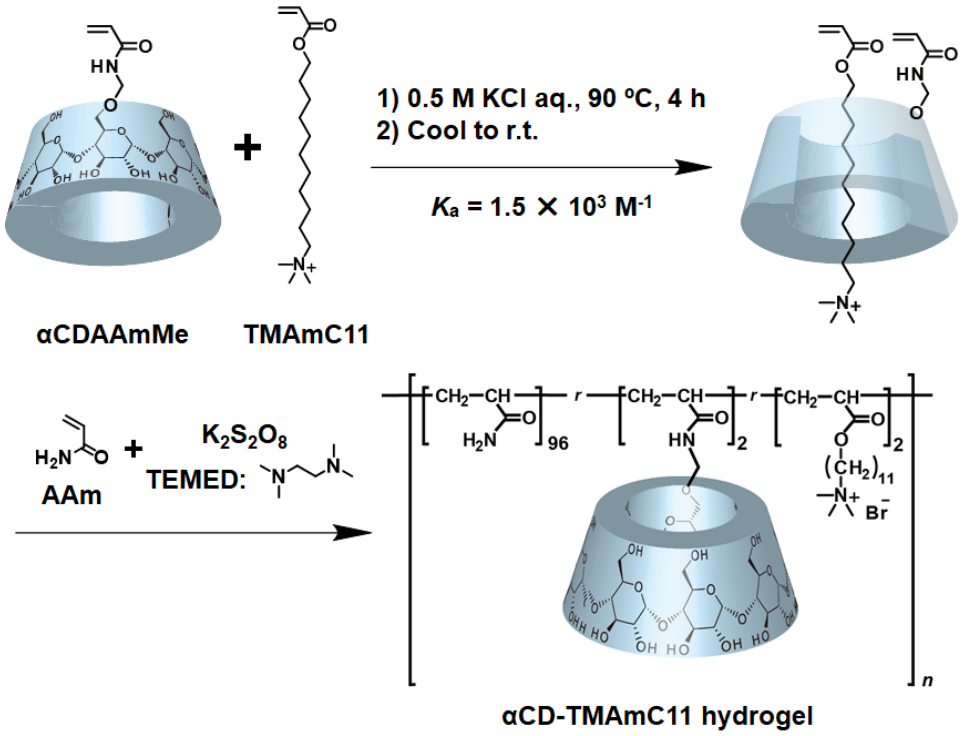

Scheme S8. Preparation of the αCD-TMAmC11 hydrogel.

αCDAAmMe (84 mg, 0.080 mmol) and TMAmC11 (29 mg, 0.080 mmol) were mixed in 0.5 M KCl aq. for 4 hours at 90 °C to form the host-guest inclusion complex. The inclusion complex of αCDAAmMe with VC11 was copolymerized with acrylamide (AAm; the main chain monomer, 273 mg, 3.84 mmol) by using a redox initiator system (11 mg (0.040 mmol) of potassium persulfate ($K_2S_2O_4$) and 4.6 mg (0.040 mmol) of *N,N,N′,N′*-tetramethylethylenediamine (TEMED)) at room temperature. The solution gelated within 5 minutes to give a self-standing hydrogel. The hydrogel were characterized by FG-MAS NMR and IR spectroscopy (see below). The amounts of reagents and the solvent use are summarized in **Table S5**.

Table S1. Amount of reagents and solvents used in the preparation of the αCD-C12 hydrogel.

	KCl aq. /mL	AAm /mg	αCDAAmMe /mg	C12 /mg	KPS /mg	TEMED /μL
αCD-C12 hydrogel	2.0	273	84.5	18.9	10.8	5.96

Table S2. Amount of reagents and solvents used in the preparation of the αCD-ImC11 hydrogel.

	KCl aq. /mL	AAm /mg	αCDAAmMe /mg	ImC11 /mg	KPS /mg	TEMED /μL
αCD-ImC11 hydrogel	2.0	273	84.5	31.0	10.8	5.96

Table S3. Amount of reagents and solvents used in the preparation of the αCD-PyC11 hydrogel.

	KCl aq. /mL	AAm /mg	αCDAAmMe /mg	PyC11 /mg	KPS /mg	TEMED /μL
αCD-PyC11 hydrogel	2.0	273	84.5	30.8	10.8	5.96

Table S4. Amount of reagents and solvents used in the preparation of the αCD-VC11 hydrogel.

	KCl aq. /mL	AAm /mg	αCDAAmMe /mg	VC11 /mg	KPS /mg	TEMED /μL
αCD-VC11 hydrogel	2.0	273	84.5	37.4	10.8	5.96

Table S5. Amount of reagents and solvents used in the preparation of the αCD-TMAmC11 hydrogel.

	KCl aq. /mL	AAm /mg	αCDAAmMe /mg	TMAmC11 /mg	KPS /mg	TEMED /μL
αCD-TMAmC11 hydrogel	2.0	273	84.5	29.1	10.8	5.96

6. Characterization of the supramolecular hydrogels

FT-IR spectra

Figures S23a–c and e show FT-IR spectra of the αCD-C12, αCD-ImC11, αCD-PyC11, and αCD-TMAmC11 hydrogels (KBr tablet method). The as-prepared αCD-R hydrogels were freeze-dried to eliminate water. The freeze-dried hydrogels were additionally dried in vacuum at 100 °C for 3 days to reduce absorption derived from water. They were analyzed in KBr pill form.

Figure S23d shows FT-IR spectrum of the freeze-dried αCD-VC11 hydrogel in attenuated total reflection (ATR) method using a diamond prism.

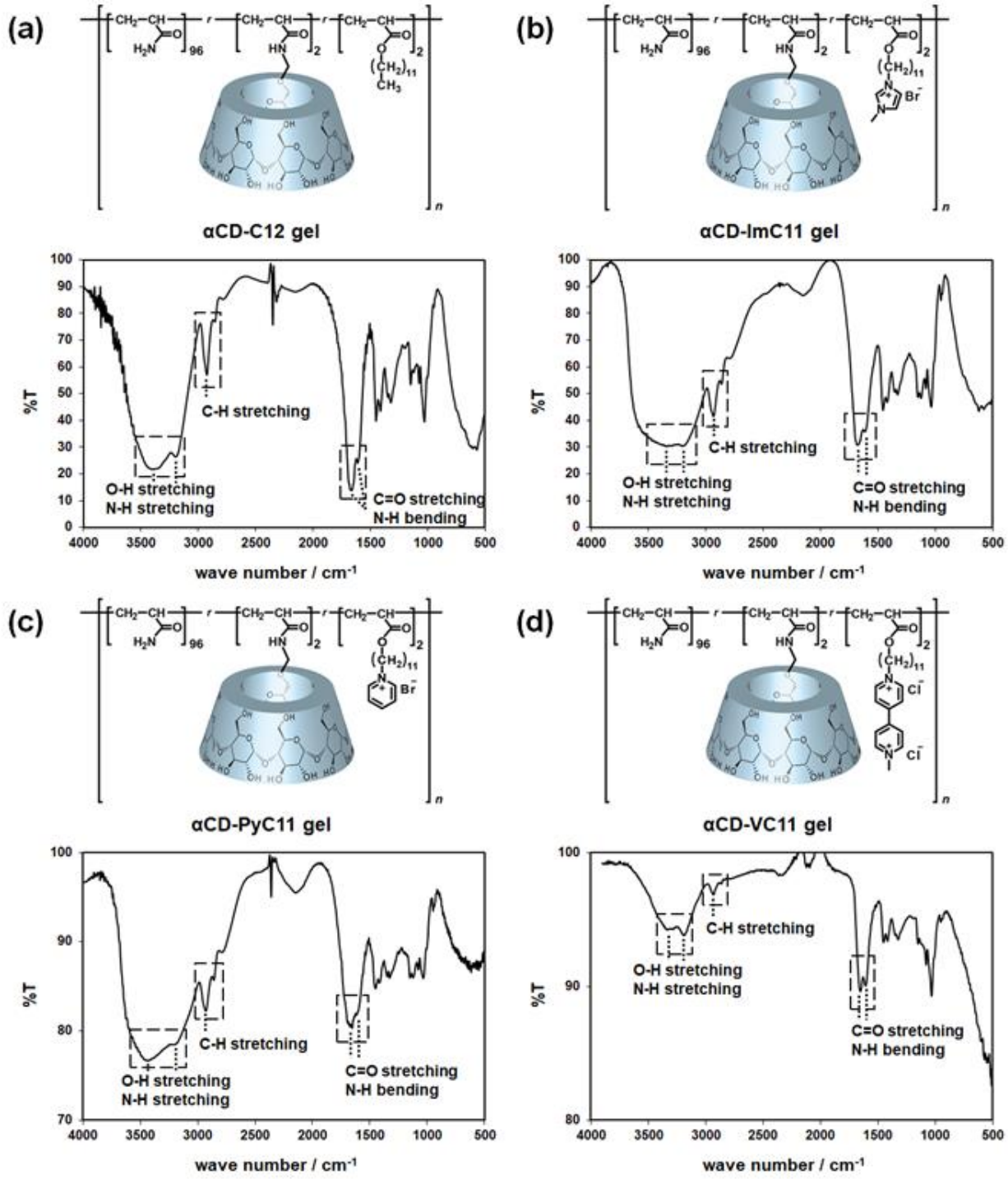

Figure S23. FT-IR spectra of **(a)** αCD-C12, **(b)** αCD-ImC11, **(c)** αCD-PyC11, **(d)** αCD-VC11, and **(e)** αCD-TMAmC11.

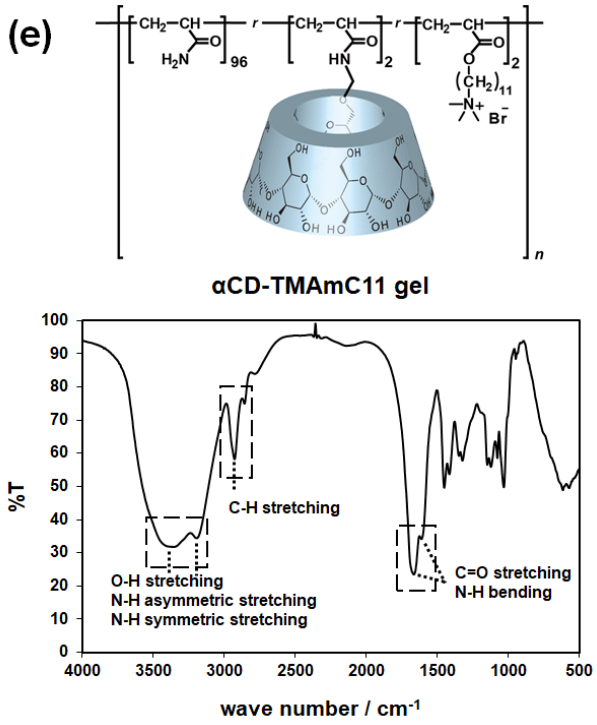

Figure S23. (Continued)

FG-MAS NMR spectra

The as-prepared αCD-R hydrogels were freeze-dried, immersed in D_2O, and analyzed by FG-MAS spectroscopy (**Figures S24–28**).

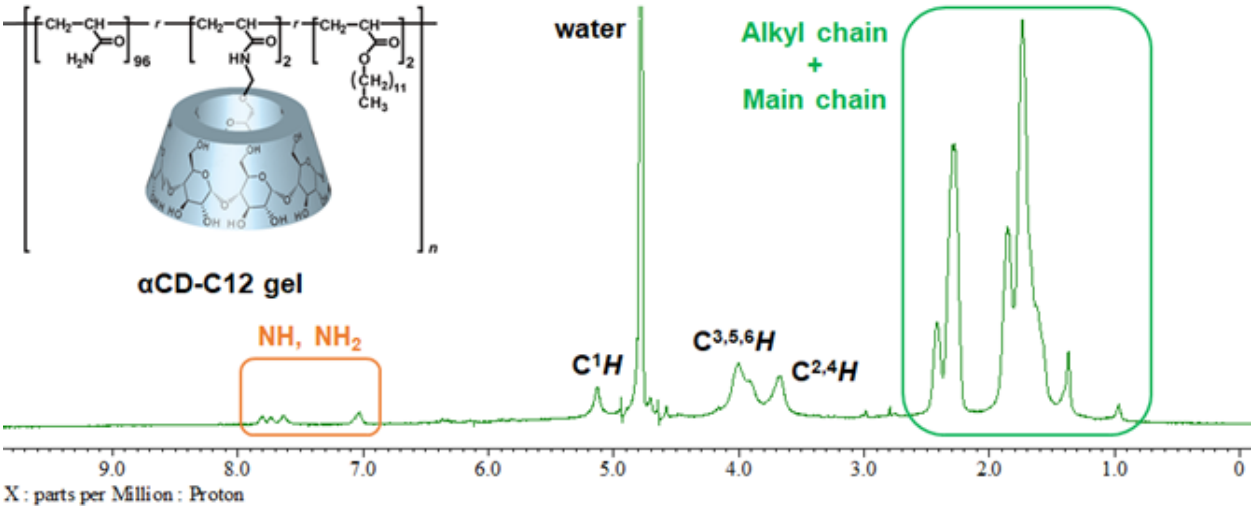

Figure S24. 400 MHz ^{1}H FG-MAS NMR spectrum of the αCD-C12 hydrogel (immersed in D_2O) at 25 °C. The frequency of the magic angle spinning was 7 kHz.

Amount of each residues
In the preparation: [αCD] / [C12] / [AAm] = 2.0 / 2.0 / 96.0.
Calculated from the spectrum: [αCD] / [C12] / [AAm] = 0.5 / 1.1 / 98.4.

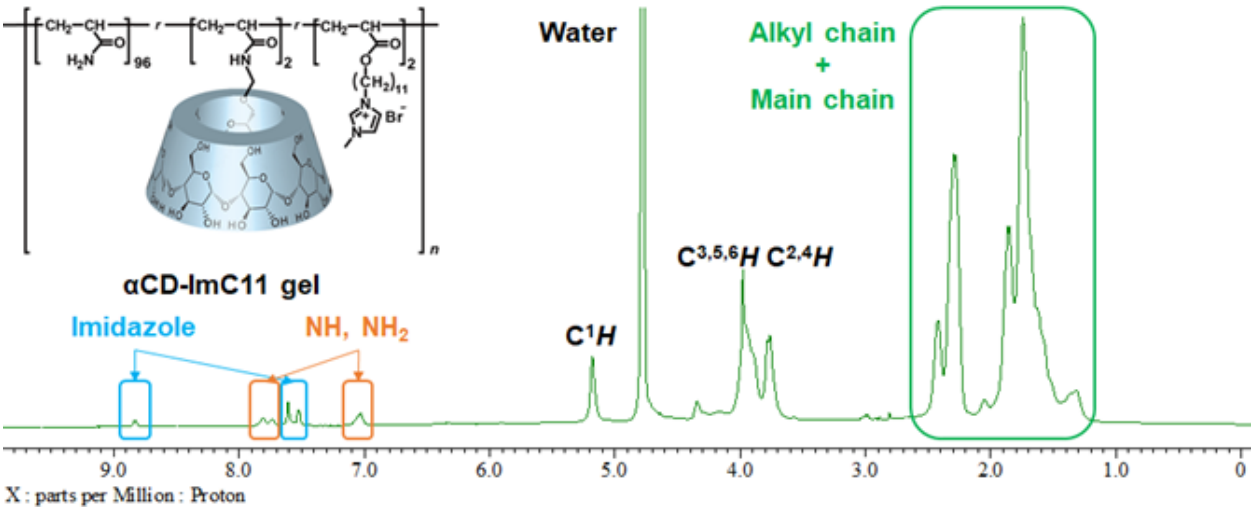

Figure S25. 400 MHz ^{1}H FG-MAS NMR spectrum of the αCD-ImC11 hydrogel (immersed in D_2O) at 25 °C. The frequency of the magic angle spinning was 7 kHz.

Amount of each residues
In the preparation: [αCD] / [ImC11] / [AAm] = 2.0 / 2.0 / 96.0.
Calculated from the spectrum: [αCD] / [ImC11] / [AAm] = 1.5 / 1.8 / 96.7.

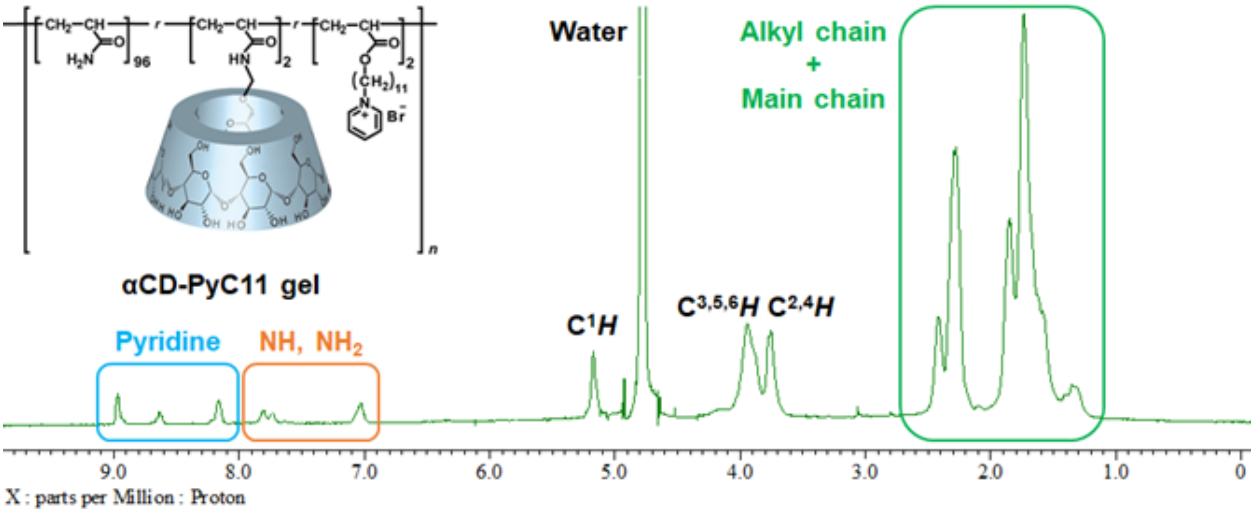

Figure S26. 400 MHz ^{1}H FG-MAS NMR spectrum of the αCD-PyC11 hydrogel (immersed in D_2O) at 25 °C. The frequency of the magic angle spinning was 7 kHz.

Amount of each residues
In the preparation: [αCD] / [PyC11] / [AAm] = 2.0 / 2.0 / 96.0.
Calculated from the spectrum: [αCD] / [PyC11] / [AAm] = 1.5 / 1.8 / 96.7.

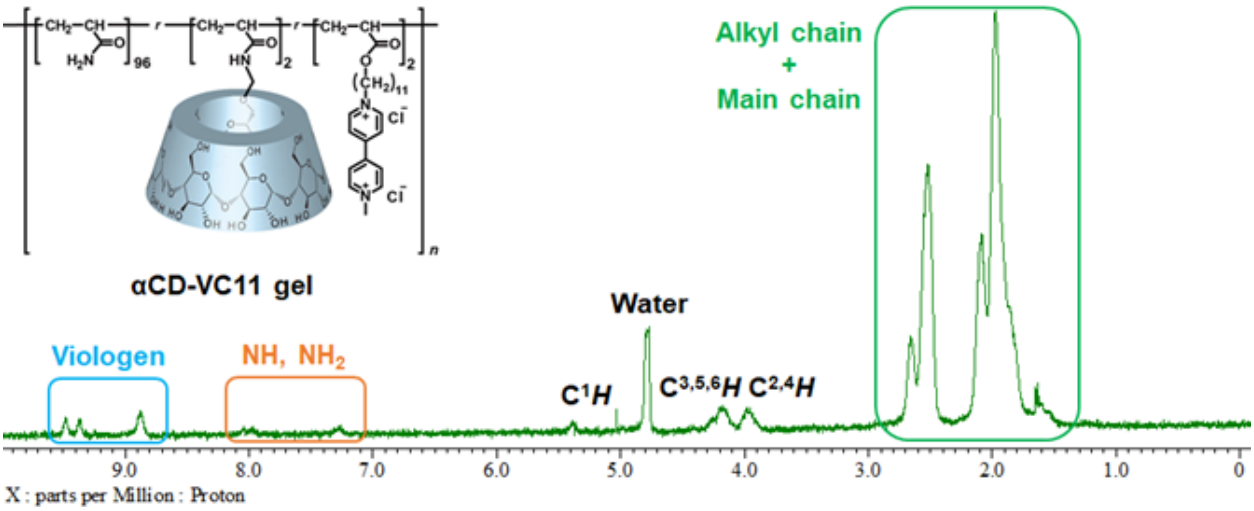

Figure S27. 400 MHz ^{1}H FG-MAS NMR spectrum of the αCD-VC11 hydrogel (immersed in D_2O) at 25 °C. The frequency of the magic angle spinning was 7 kHz.

Amount of each residues
In the preparation: [αCD] / [VC11] / [AAm] = 2.0 / 2.0 / 96.0.
Calculated from the spectrum: [αCD] / [VC11] / [AAm] = 2.1 / 2.0 / 95.9.

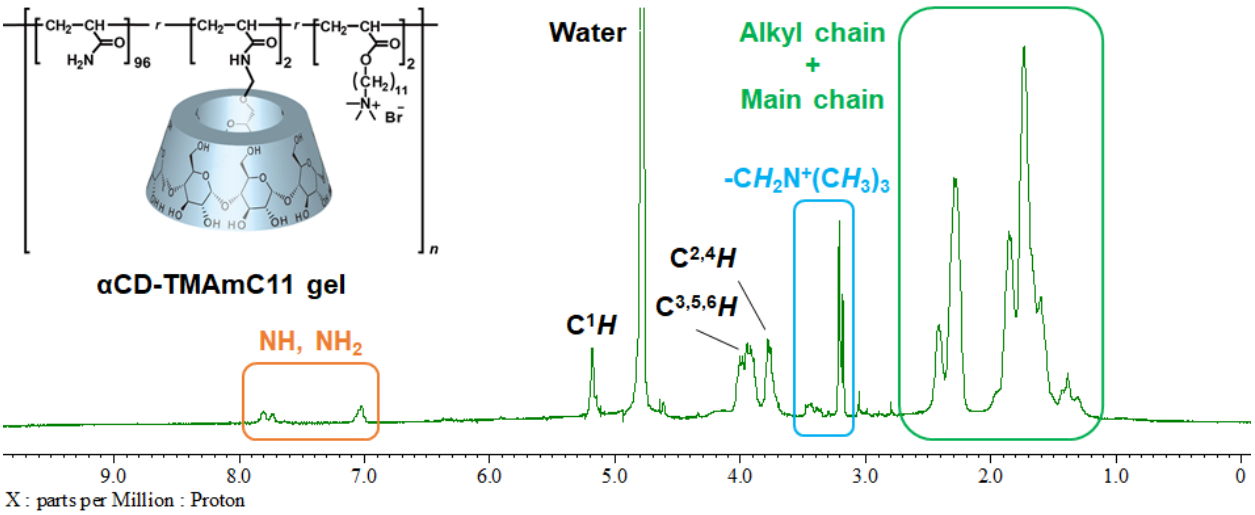

Figure S28. 400 MHz ^{1}H FG-MAS NMR spectrum of the αCD-TMAmC11 hydrogel (immersed in D_2O) at 25 °C. The frequency of the magic angle spinning was 7 kHz.

Amount of each residues
In the preparation: [αCD] / [TMAmC11] / [AAm] = 2.0 / 2.0 / 96.0.
Calculated from the spectrum: [αCD] / [TMAmC11] / [AAm] = 1.4 / 1.9 / 96.7.

7. Results of tensile test of the αCD-R hydrogels

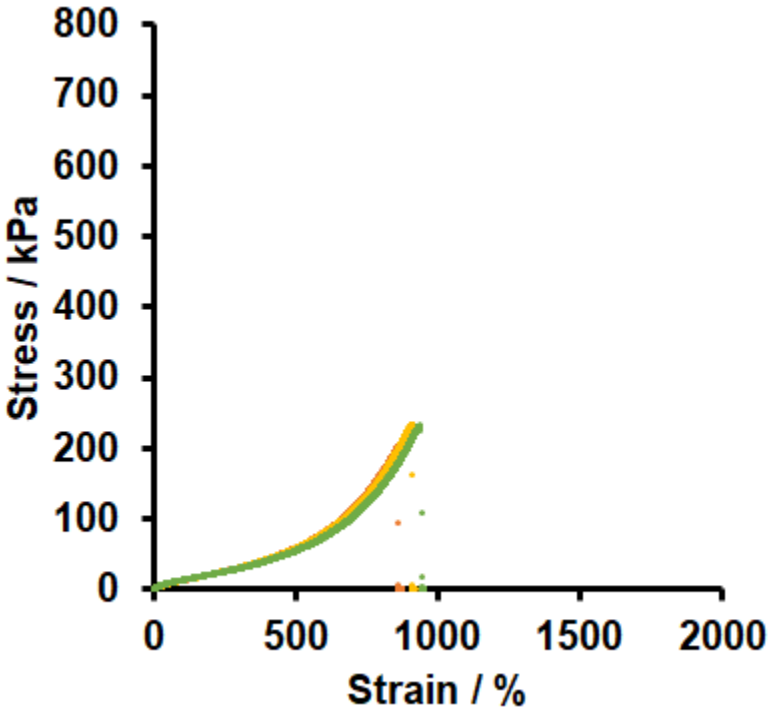

Figure S29. Stress-strain curves of the αCD-C12 hydrogel at 25 ºC at a tensile rate of 1.0 mm/s.

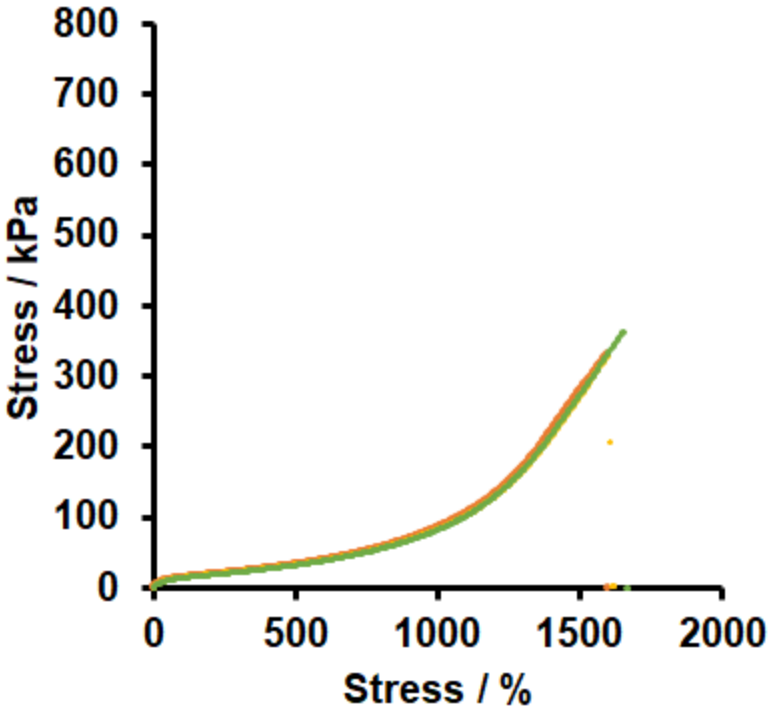

Figure S30. Stress-strain curves of the αCD-ImC11 hydrogel at 25 ºC at a tensile rate of 1.0 mm/s.

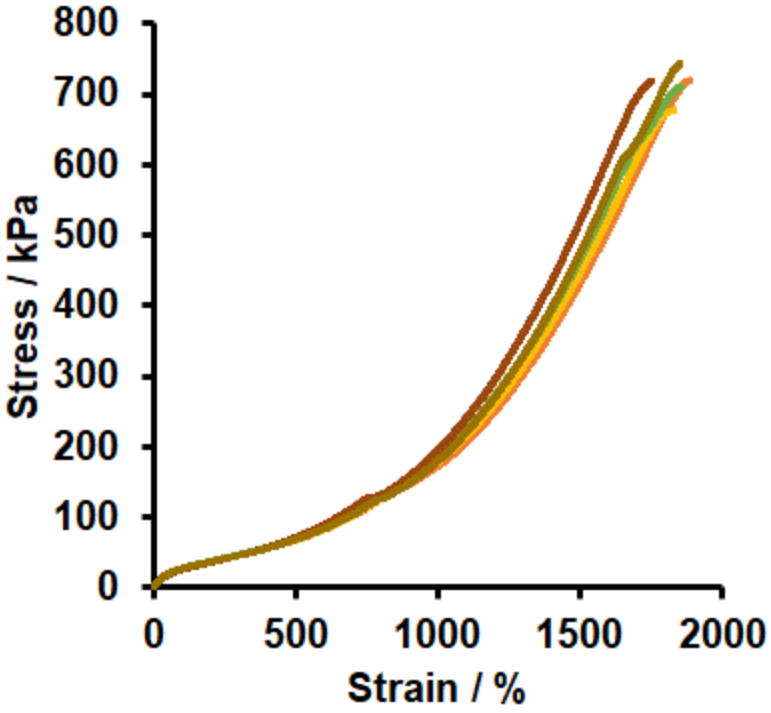

Figure S31. Stress-strain curves of the αCD-PyC11 hydrogel at 25 ºC at a tensile rate of 1.0 mm/s.

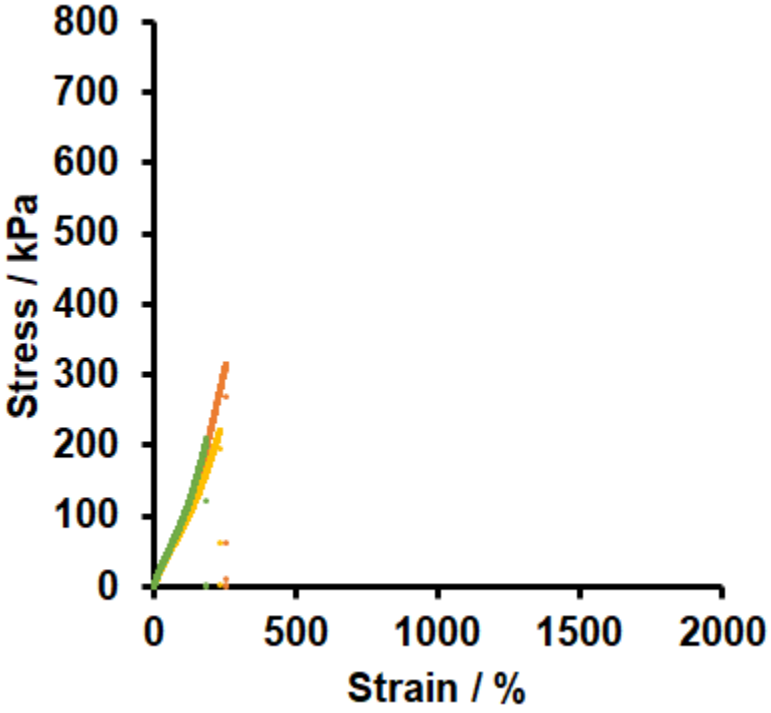

Figure S32. Stress-strain curves of the αCD-VC11 hydrogel at 25 ºC at a tensile rate of 1.0 mm/s.

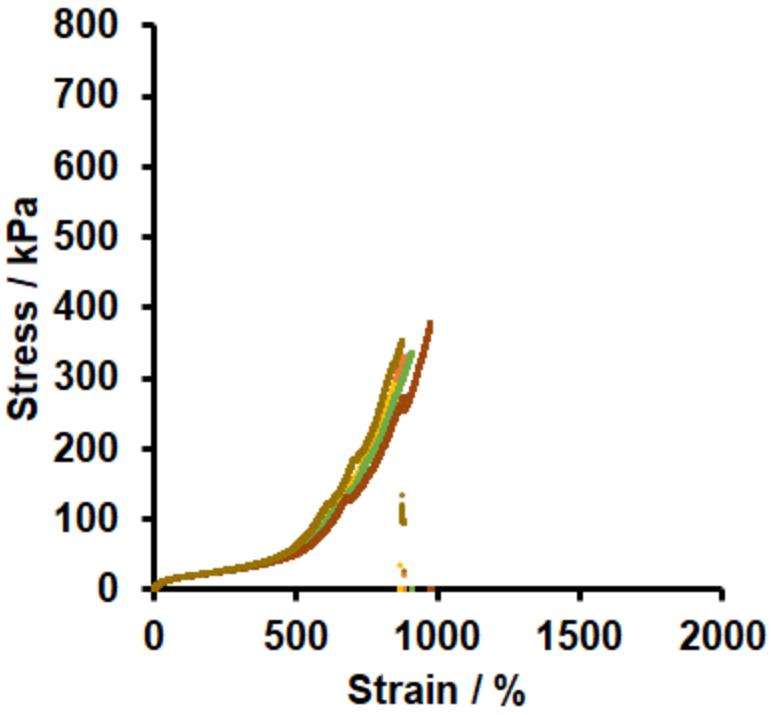

Figure S33. Stress-strain curves of the αCD-PyC11 hydrogel at 25 ºC at a tensile rate of 0.10 mm/s.

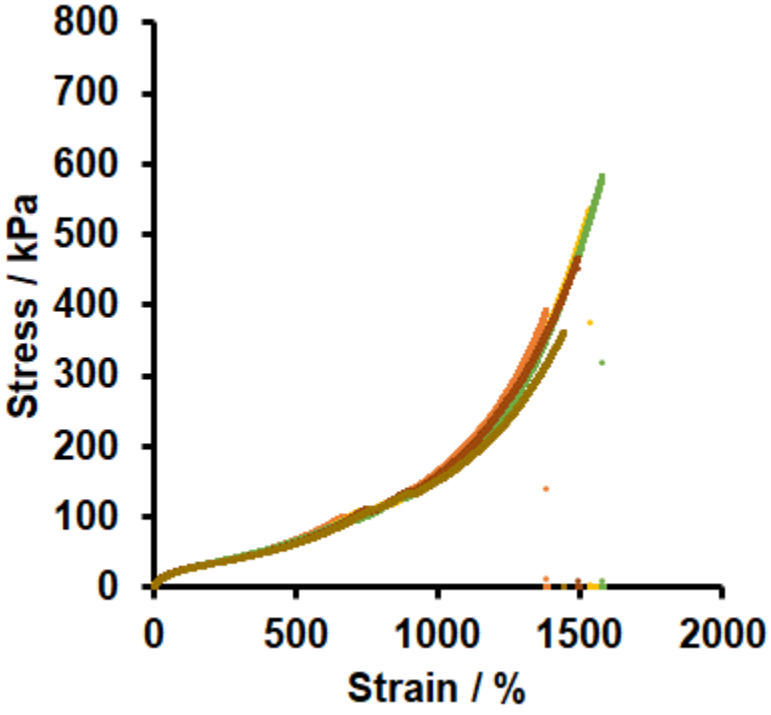

Figure S34. Stress-strain curves of the αCD-PyC11 hydrogel at 25 ºC at a tensile rate of 0.50 mm/s.

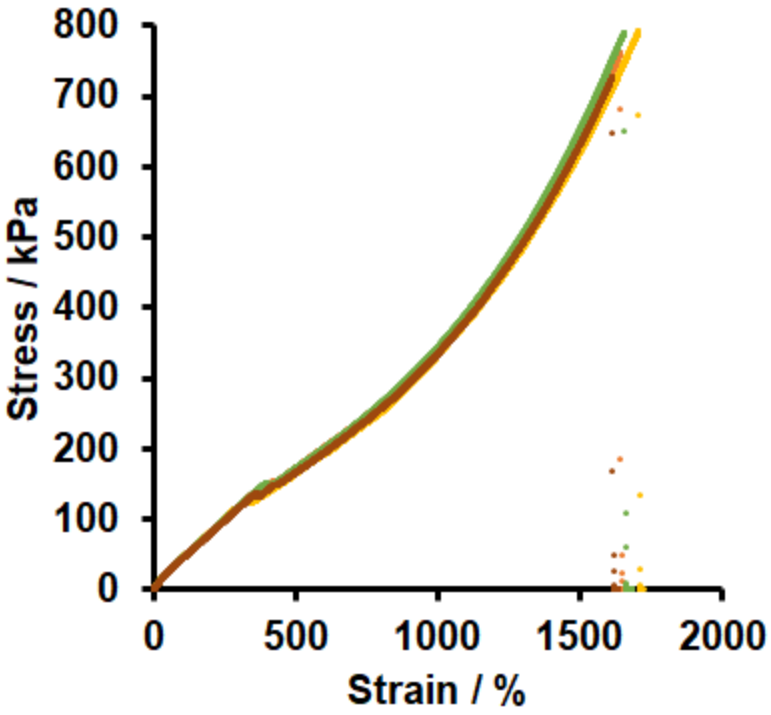

Figure S35. Stress-strain curves of the αCD-PyC11 hydrogel at 25 ºC at a tensile rate of 10 mm/s.

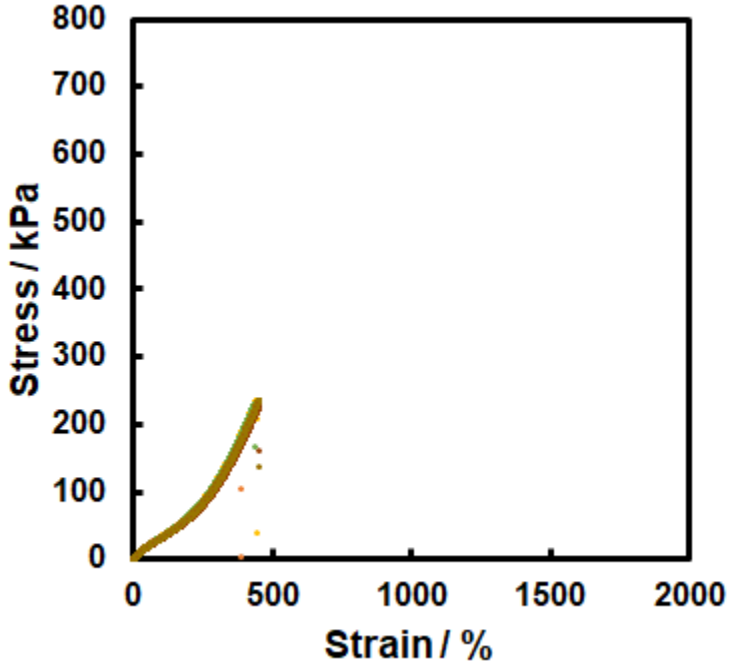

Figure S36. Stress-strain curves of the αCD-TMAmC11 hydrogel at 25 ºC at a tensile rate of 1.0 mm/s.

8. Quantum chemical calculations of guest monomers

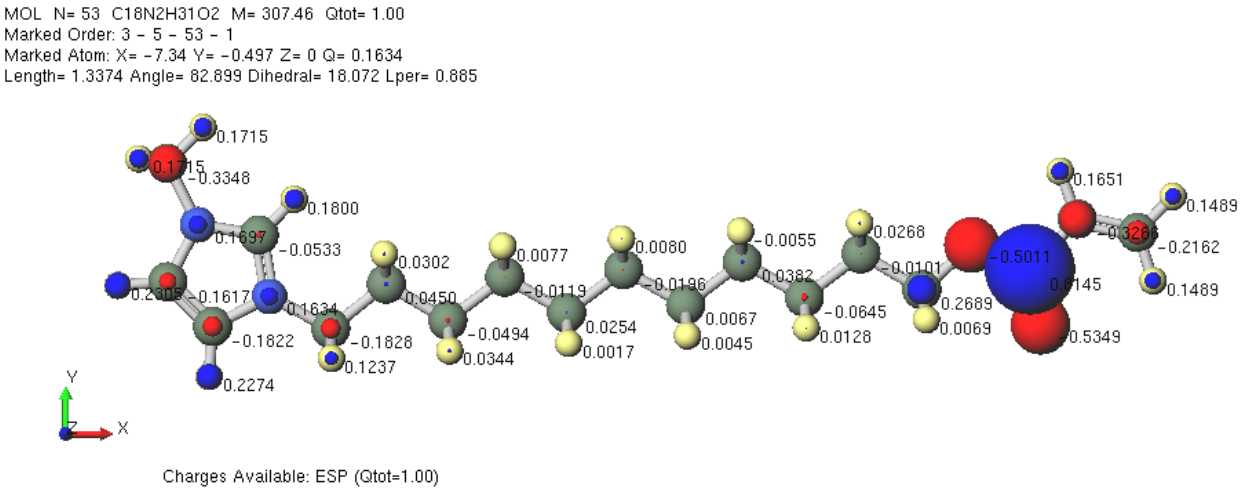

Figure S37. The RESP partial atomic charges in ImC11 monomer.

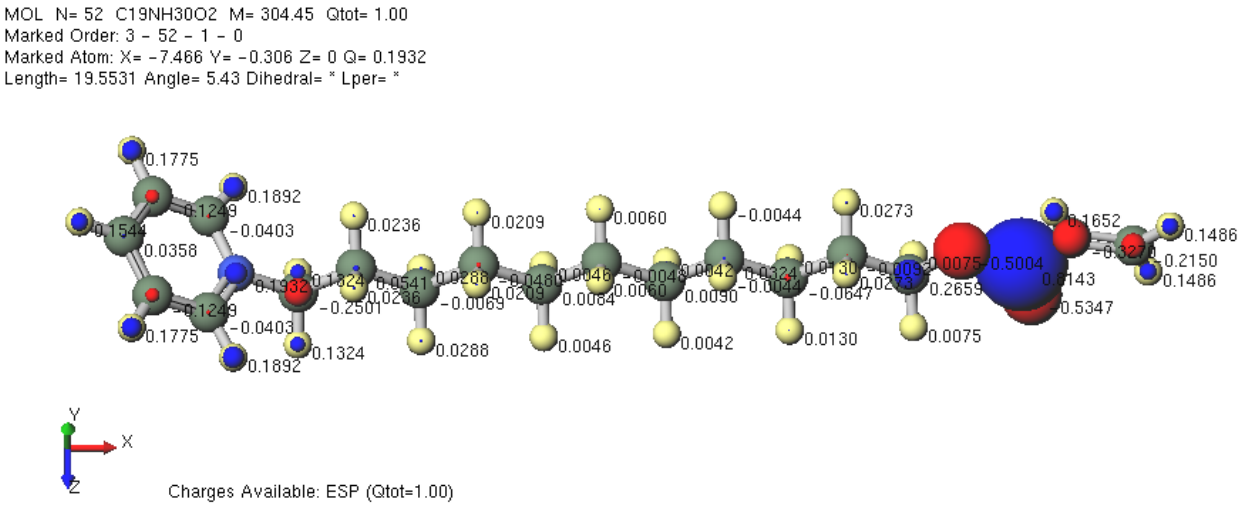

Figure S38. The RESP partial atomic charges in PyC11 monomer.

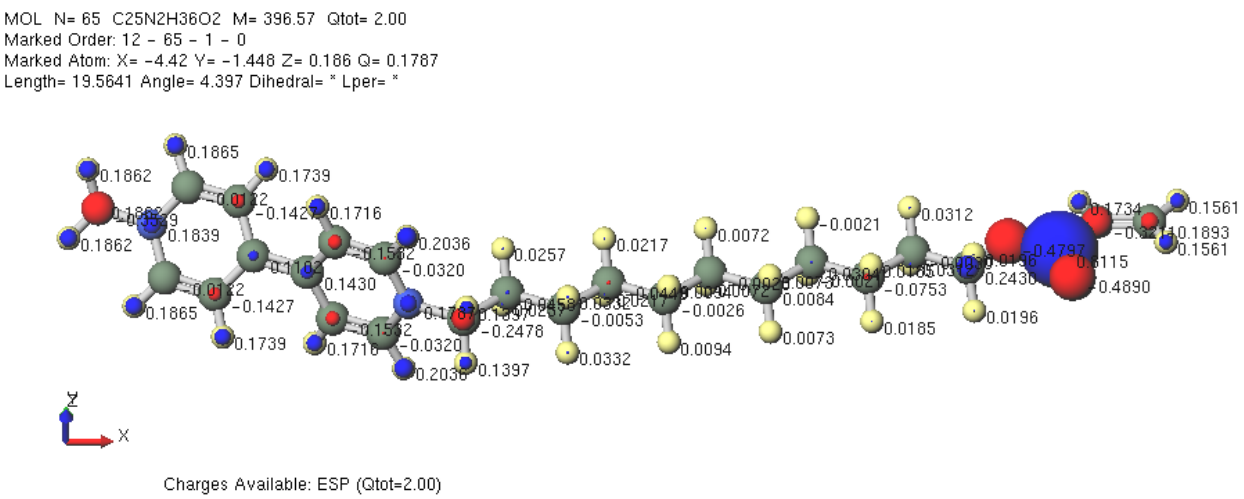

Figure S39. The RESP partial atomic charges in VC11 monomer.

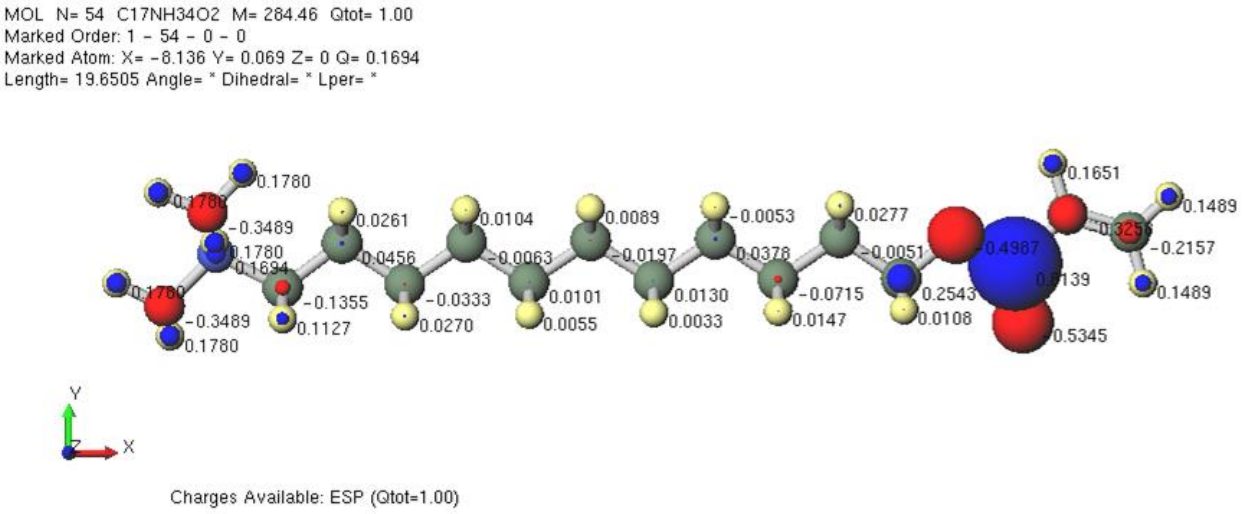

Figure S40. The RESP partial atomic charges in TMAmC11 monomer.

9. Linear viscoelastic measurement of the αCD-R hydrogels

Dynamic viscoelastic measurements of sheet-like samples with thickness of ~ 1 mm were performed with an Anton Paar MCR302 rheometer. Angular frequency (ω) sweep from 0.1 to 100 rad/s was performed using the parallel-plate fixture with 8 mm in diameter in a temperature range of 0–45 °C. The oscillatory shear strain amplitudes for all the tests were within the range of linear viscoelasticity. Results of the αCD-R hydrogel at different temperatures and frequencies followed the time-temperature superposition principle. **Figures S41–S45** show the master curves of storage modulus (G'), loss modulus (G'') and loss factor (tanδ) referenced at 25 °C and the Arrhenius plot depicting the temperature dependence of the shift factors (a_T) for each sample. Relaxation modulus (ΔG) and second-order average relaxation times ($<\tau>_w$) were estimated by fitting master curves of G' and G'' with the generalized Maxwellian model, except for the αCD-C12, αCD-VC11, and αCD-TMAmC11 hydrogels.

$$G' = \sum_{p\geq 1}^{N} G_p \frac{\omega^2 {\tau_p}^2}{1 + \omega^2 {\tau_p}^2} + G_N \tag{4}$$

$$G'' = \sum_{p\geq 1}^{N} G_p \frac{\omega \tau_p}{1 + \omega^2 {\tau_p}^2} \tag{5}$$

$$\Delta G = \sum_{p\geq 1}^{N} G_p \tag{6}$$

$$\langle \tau \rangle_w = \frac{\sum_{p\geq 1}^{N} G_p {\tau_p}^2}{\sum_{p\geq 1}^{N} G_p \tau_p} \tag{7}$$

G_p: Relaxation strength in p^{th} relaxation mode.

τ_p: Relaxation time in p^{th} relaxation mode.

G_N: Terminal modulus.

The apparent activation energy ΔE_a was calculated from Arrhenius equation (8), where a_T was the shift factor, R was the ideal gas constant, and A was a constant.

$$a_T = Ae^{-\frac{\Delta E_a}{RT}} \quad (8)$$

The equation (8) was converted to equation (9). **Figures S41e-45e** shows Arrhenius plots of logarithm of a_T and inverse of T using eq. (9).

$$\ln a_T = \frac{\Delta E_a}{R}\left(\frac{1}{T} - \frac{1}{T_0}\right) \quad (9)$$

In **Figures S41d–45d**, the plateau values from entanglements (G_e) and reversible crosslinks (host-guest crosslinks) with entanglements (G_s) are shown as dotted and dashed lines, respectively. G_e was experimentally estimated to be about 5.0×10^3 Pa from the rubbery plateau level of G' for the entangled polyacrylamide solution.[6] G_s was calculated with a following equation (10), where v_s was the number density of temporary cross-linking points (stickers) and k_B was Boltzmann constant.[6,7]

$$G_s = v_s k_B T + G_e \quad (10)$$

Assuming that all the inclusion complexes in the αCD-R hydrogel acted as stickers, we roughly estimated G_s to be about $9.1–9.6 \times 10^4$ Pa at 25 °C, based on the concentration of αCDAAmMe and guest monomer, and K_a. The observed G' of the αCD-R hydrogel showed decay from G_s and G_e, indicating that observed relaxation modes resulted from association and dissociation of inclusion complexes. These characteristics are consistent with sticky reptation model, which considers that the stickers retard the global diffusion of the entangled chains (reptation). This consistence indicates that the αCD-R hydrogels are the entanglement-dominant networks with sticky points. It should be noted that the level of G_s does not agree with the plateau modulus at high frequency limit. This deviation is attributed to connectivity defects including intramolecular connection, which does not contribute to elasticity.

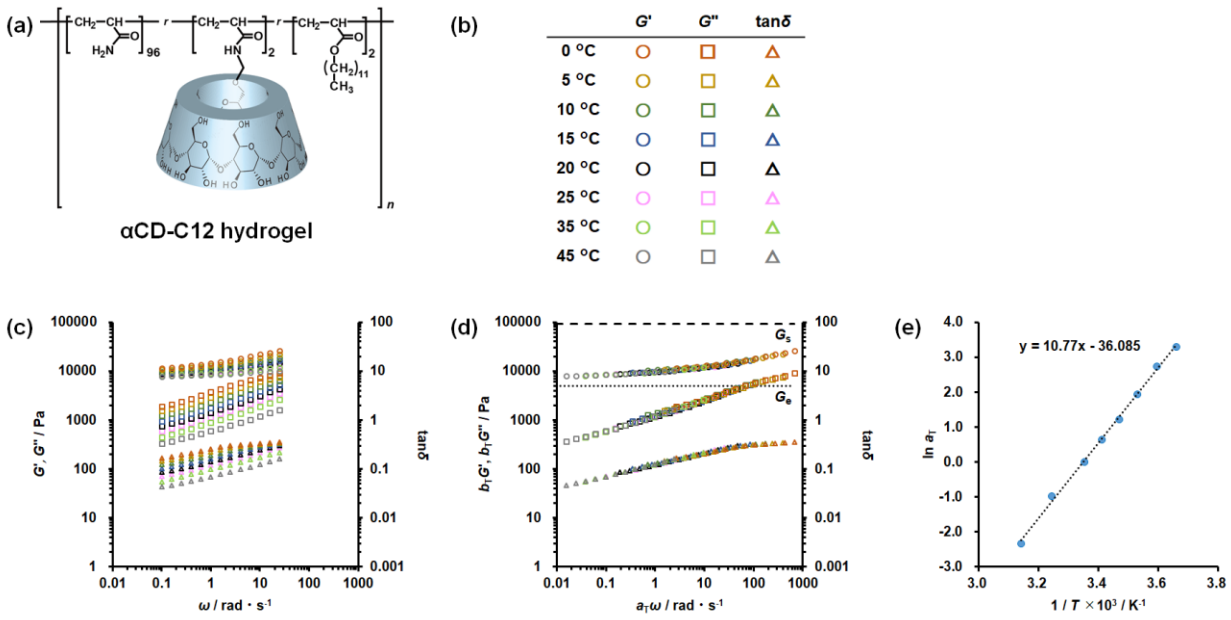

Figure S41. (a) Chemical structure of the αCD-C12 hydrogel. **(b)** Symbols for G', G'', and tanδ defined at each temperature. **(c)** Angular frequency dependence of G', G'', and tanδ. **(d)** Master curves of G', G'', and tanδ of the αCD-C12 hydrogel referenced at 25 °C. **(e)** The Arrhenius plot of a_T.

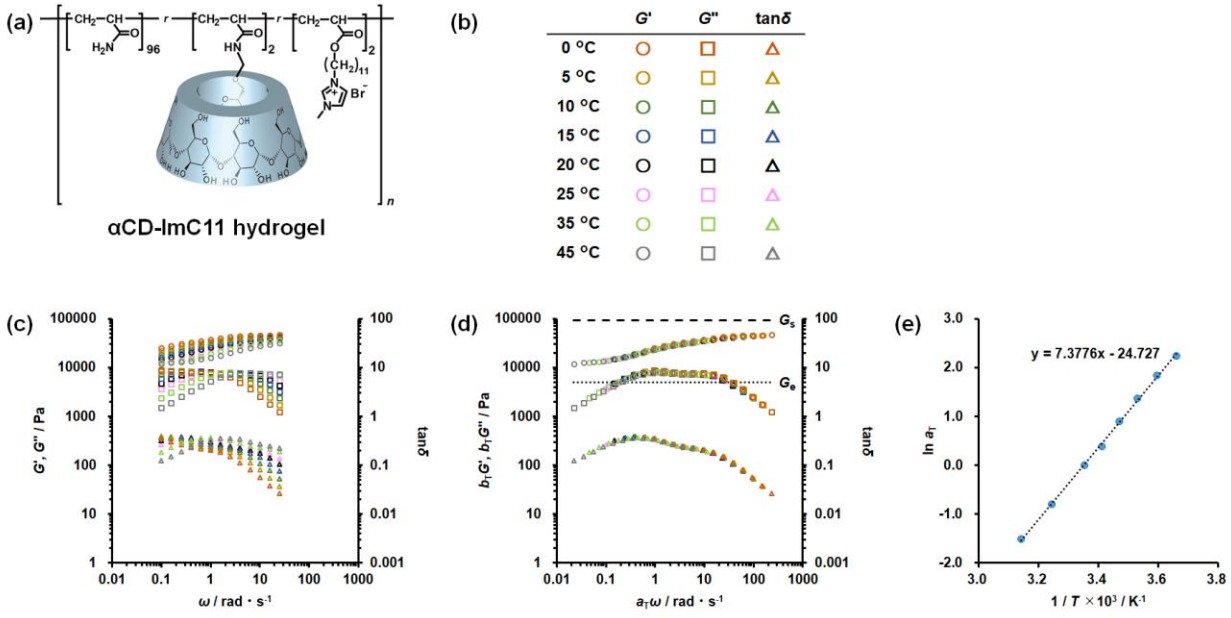

Figure S42. (a) Chemical structure of the αCD-ImC11 hydrogel. **(b)** Symbols for G', G'', and tanδ defined at each temperature. **(c)** Angular frequency dependence of G', G'', and tanδ. **(d)** Master curves of G', G'', and tanδ of the αCD-ImC11 hydrogel referenced at 25 °C. **(e)** The Arrhenius plot of a_T.

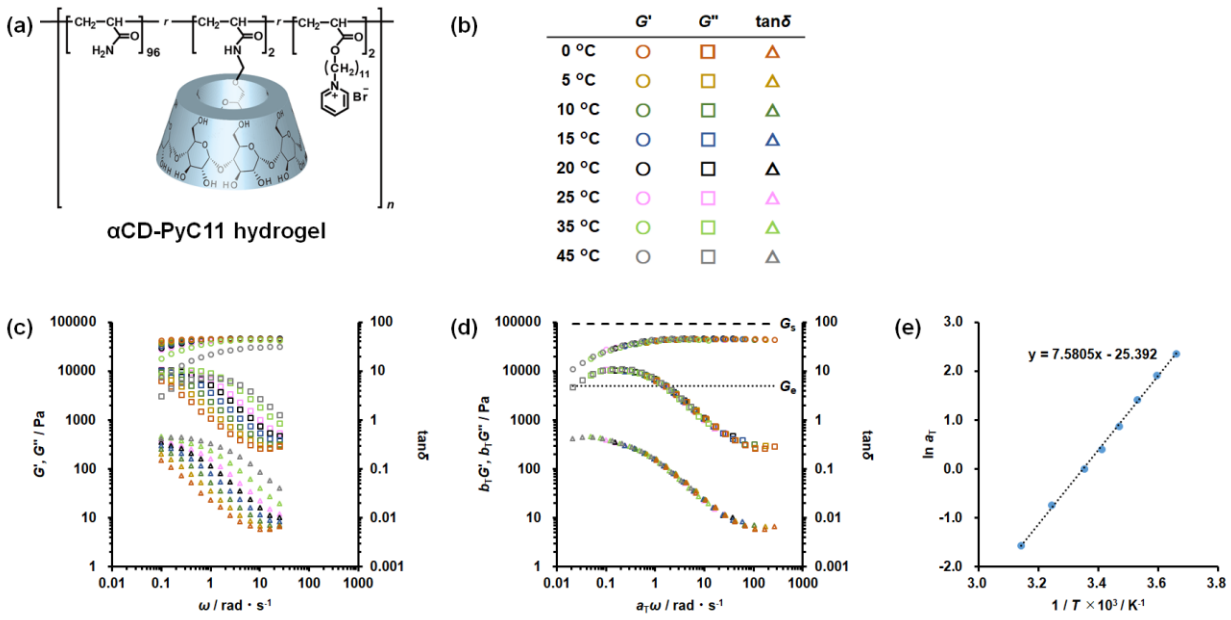

Figure S43. (a) Chemical structure of the αCD-PyC11 hydrogel. **(b)** Symbols for G', G'' and tanδ defined at each temperature. **(c)** Angular frequency dependence of G', G'', and tanδ. **(d)** Master curves of G', G'', and tanδ of the αCD-PyC11 hydrogel referenced at 25 °C. **(e)** The Arrhenius plot of a_T.

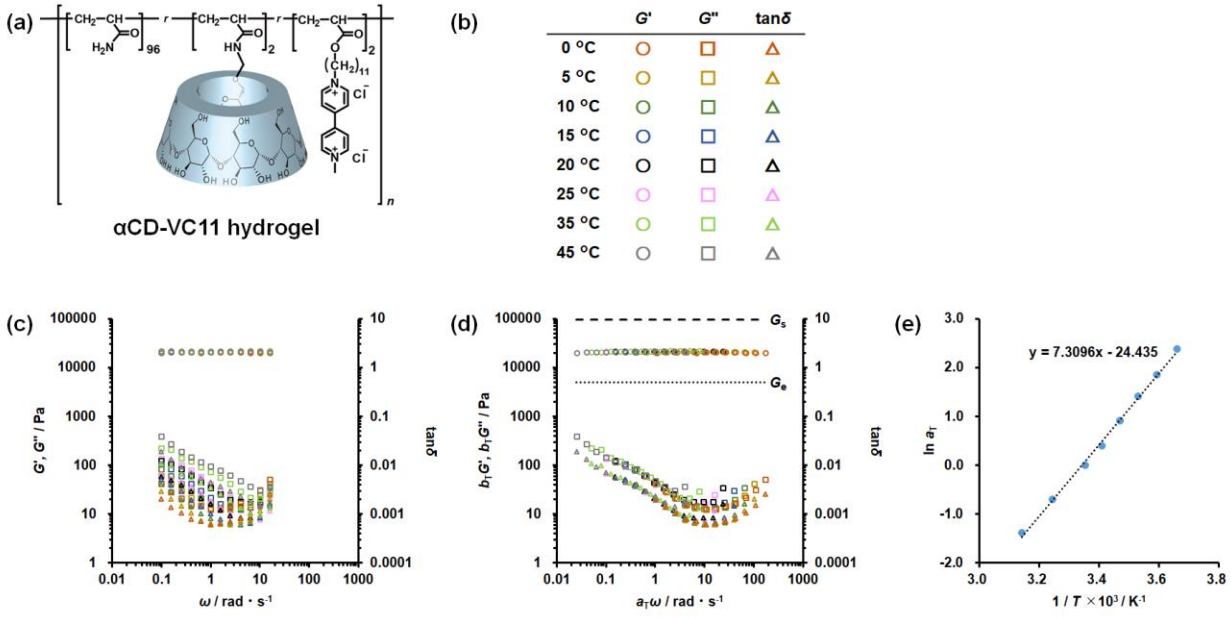

Figure S44. (a) Chemical structure of the αCD-VC11 hydrogel. **(b)** Symbols for G', G'', and tanδ defined at each temperature. **(c)** Angular frequency dependence of G', G'', and tanδ. **(d)** Master curves of G', G'', and tanδ of the αCD-VC11 hydrogel referenced at 25 °C. **(e)** The Arrhenius plot of a_T.

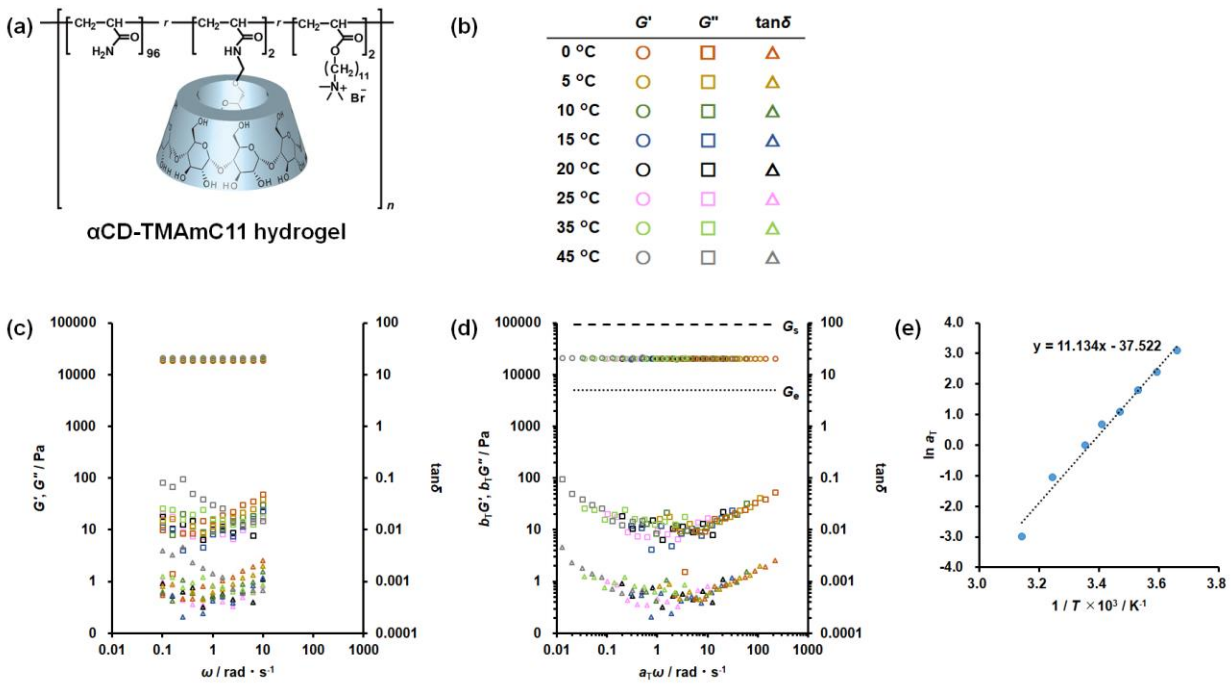

Figure S45. (a) Chemical structure of the αCD-TMAmC11 hydrogel. **(b)** Symbols for G', G'', and tanδ defined at each temperature. **(c)** Angular frequency dependence of G', G'', and tanδ. **(d)** Master curves of G', G'', and tanδ of the αCD-TMAmC11 hydrogel referenced at 25 °C. **(e)** The Arrhenius plot of a_T.

To detect relaxation time of the αCD-VC11 hydrogel, stress-relaxation tests were performed with the rheometer MCR302 (**Figure S46**). The relaxation modulus ($G(t)$) was fitted with the following equation using seven relaxation modes (**Table S6**).

$$G(t) = \sum_{p\geq 1}^{N} G_p e^{-\frac{t}{\tau_p}} + G_{\mathrm{N}} \tag{11}$$

Based on obtained parameters, we deduced the complex moduli (**Figure S47**). Calculated values, especially G', agrees with the experimentally obtained complex moduli, indicating that the stress relaxation tests successfully performed in the linear viscoelastic range. $<\tau>_{\mathrm{w}}$ was calculated as 6.6 $\times 10^3$ s with equation (7).

Table S6. Parameters G_{p} and τ_{p} used for curve fitting of the αCD-VC11 hydrogel.

mode	1	2	3	4	5	6	7	G_{N}
G_{p} / Pa	3256	2497	4137	4491	1658	1198	414	7964
τ_{p} / s	1309	1350	5255	7099	7698	9006	10089	-

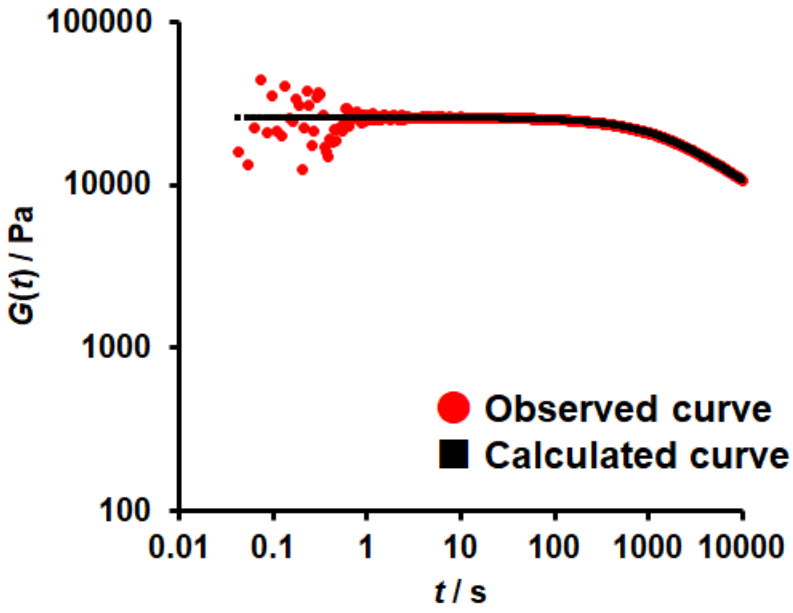

Figure S46. Stress-relaxation curves of the αCD-VC11 hydrogel (γ = 0.4%, T = 25 °C).

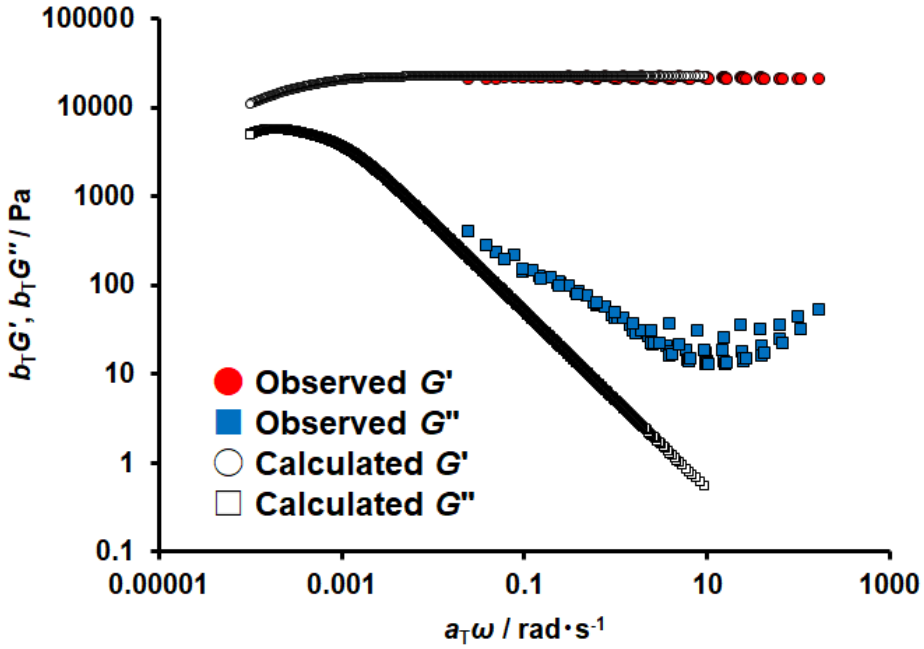

Figure S47. The comparison between calculated moduli and master curves of G' and G'' of the αCD-VC11 hydrogel.

For the same reason, stress-relaxation test of the αCD-TMAmC11 hydrogel was performed (**Figures S48 and S49, Table S7**). The result was fitted with equation (11) using a relaxation mode and $<\tau>_w$ was calculated as 9.5×10^3 s with equation (7).

Table S7. Parameters G_p and τ_p used for curve fitting of the αCD-TMAmC11 hydrogel.

mode	1	2	3	4	5	6	7	G_N
G_p / Pa	16899	-	-	-	-	-	-	-
τ_p / s	9455	-	-	-	-	-	-	-

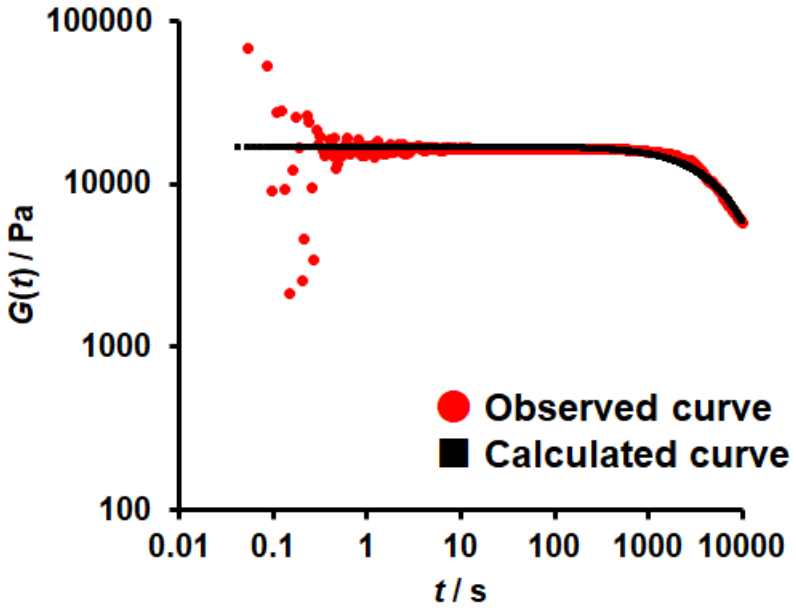

Figure S48. Stress-relaxation curves of the αCD-TMAmC11 hydrogel (γ = 0.6%, T = 25 °C).

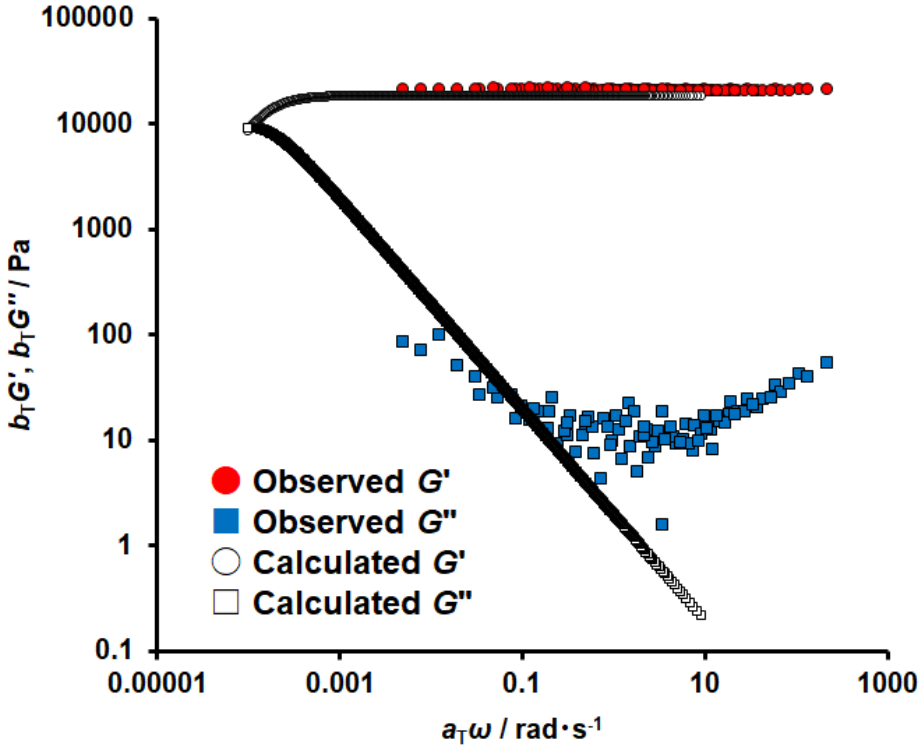

Figure S49. The comparison between calculated moduli and master curves of G' and G'' of the αCD-TMAmC11 hydrogel.

As shown in **Figures S50–55** and **Table S8–10**, stress-relaxation tests of the αCD-C12, αCD-ImC11, and αCD-PyC11 hydrogels were similarly performed in the linear viscoelastic range. These $G(t)$ monotonically decreased, and the calculated G' reached the secondary rubbery plateau region in the range of $\omega \leqq 0.1$ rad/s. These low plateau moduli were about 5.1–9.5 × 10^3 Pa and correspond to the plateau modulus derived from the entangled polymer strand (G_e). On the other hand, as described above, the plateau moduli in high ω region were originating from the temporary cross-linked polymer network (G_s). These viscoelastic properties of the αCD-R hydrogels supports that the relaxation characteristics of the αCD-R hydrogels are well explained by the sticky reptation model.

Table S8. Parameters G_p and τ_p used for curve fitting of the αCD-C12 hydrogel.

mode	1	2	3	4	5	6	7	G_N
G_p / Pa	1200	702.0	392.3	188.6	-	-	-	3008
τ_p / s	2.573	21.62	226.0	3994	-	-	-	-

Table S9. Parameters G_p and τ_p used for curve fitting of the αCD-ImC11 hydrogel.

mode	1	2	3	4	5	6	7	G_N
G_p / Pa	12361	13827	3984	1305	-	-	-	9511
τ_p / s	0.1520	1.464	13.04	432.8	-	-	-	-

Table S10. Parameters G_p and τ_p used for curve fitting of the αCD-PyC11 hydrogel.

mode	1	2	3	4	5	6	7	G_N
G_p / Pa	16141	12477	4111	2704	-	-	-	5156
τ_p / s	3.714	22.28	157.8	2384	-	-	-	-

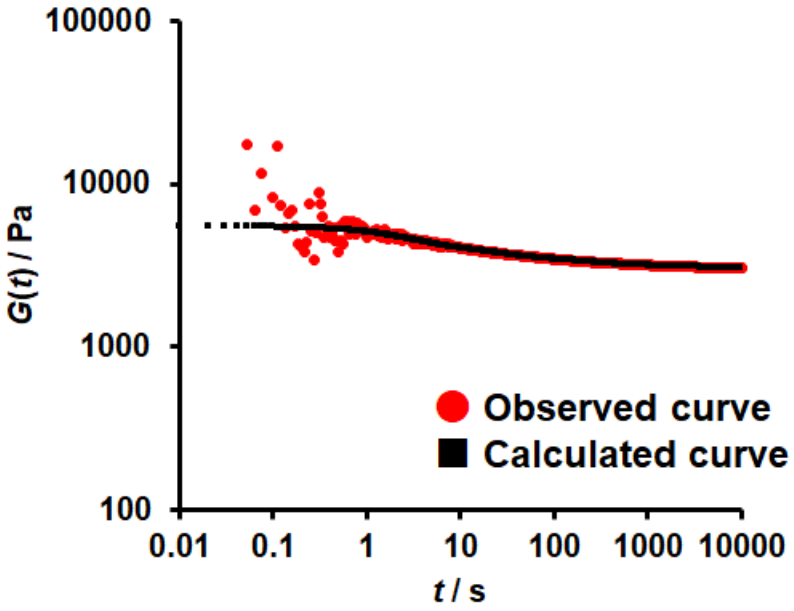

Figure S50. Stress-relaxation curves of the αCD-C12 hydrogel (γ = 3%, T = 25 °C).

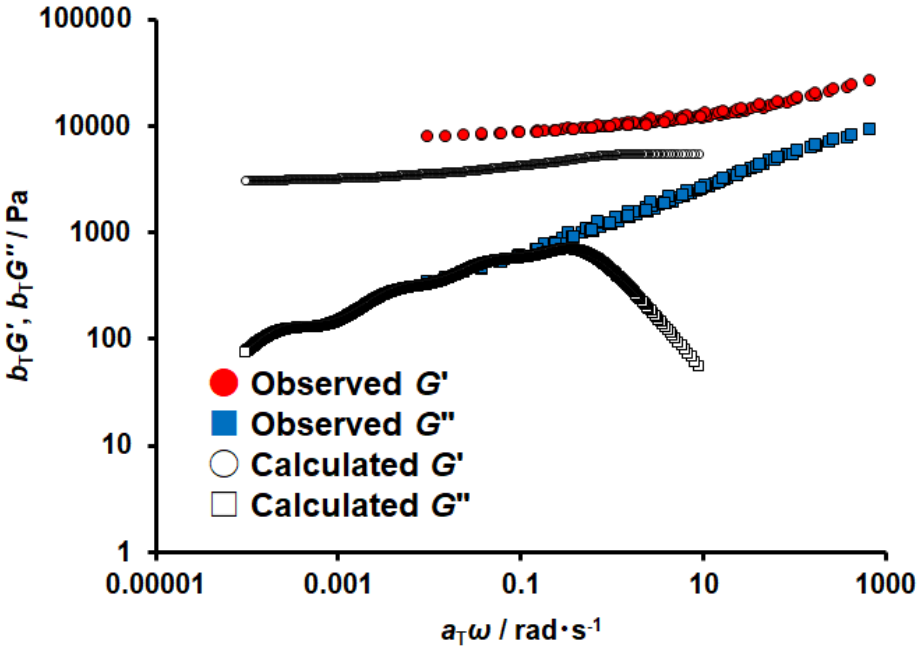

Figure S51. The comparison between calculated moduli and master curves of G' and G'' of the αCD-C12 hydrogel.

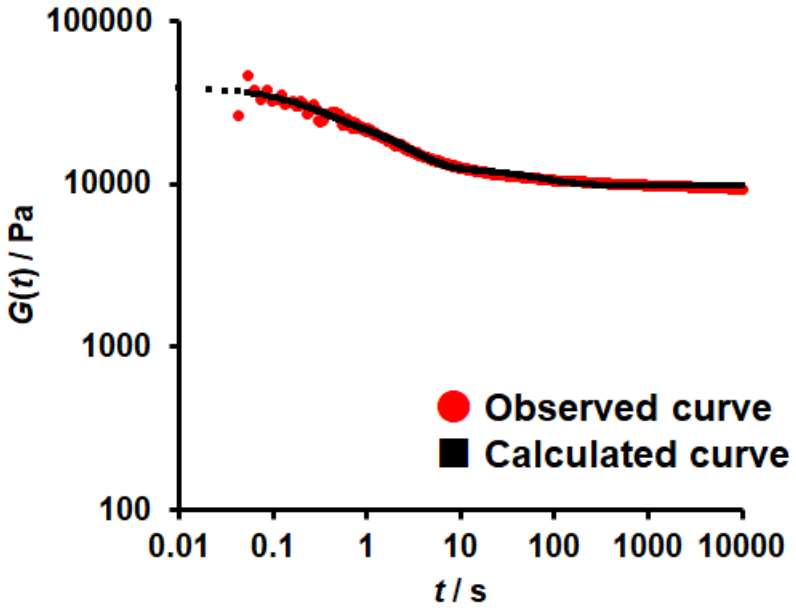

Figure S52. Stress-relaxation curves of the αCD-ImC11 hydrogel (γ = 3%, T = 25 °C).

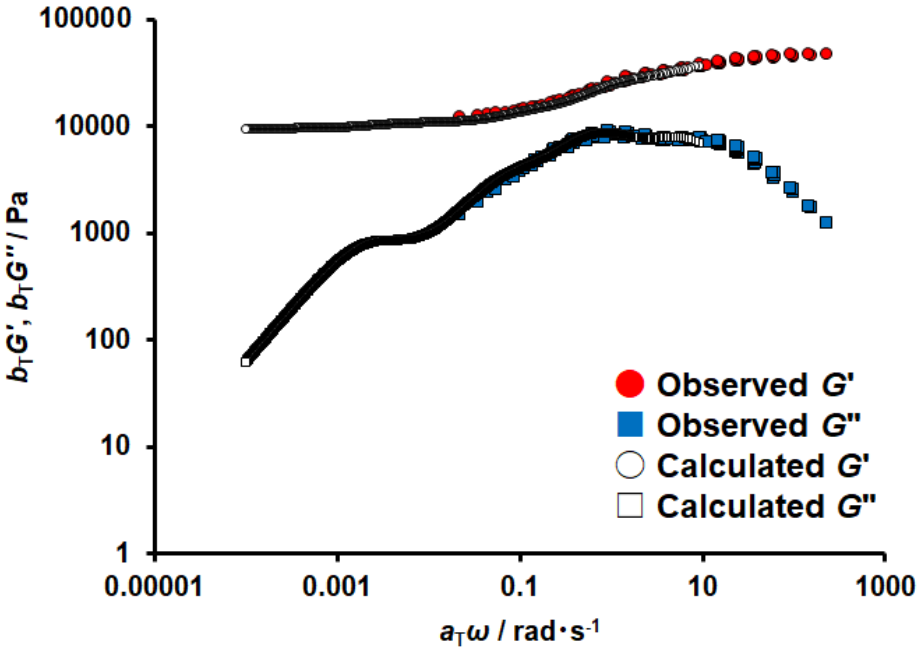

Figure S53. The comparison between calculated moduli and master curves of G' and G'' of the αCD-ImC11 hydrogel.

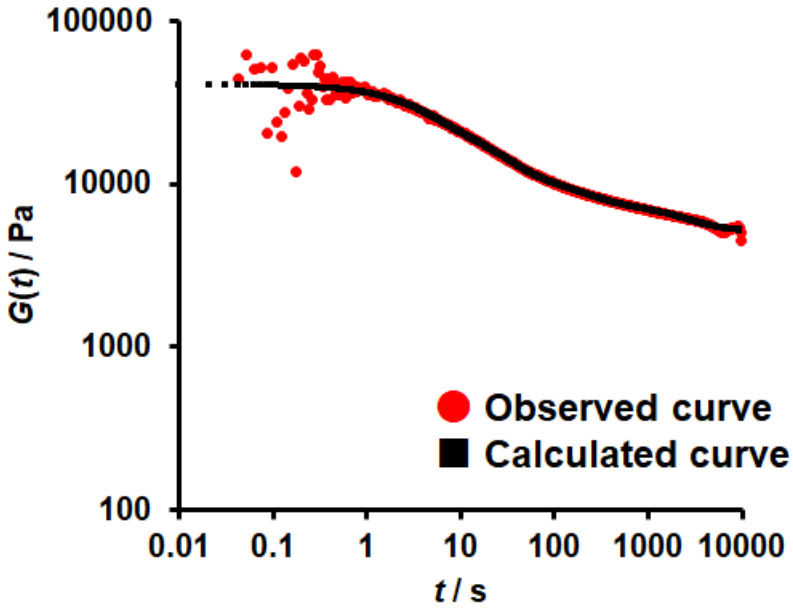

Figure S54. Stress-relaxation curves of the αCD-PyC11 hydrogel (γ = 3%, T = 25 °C).

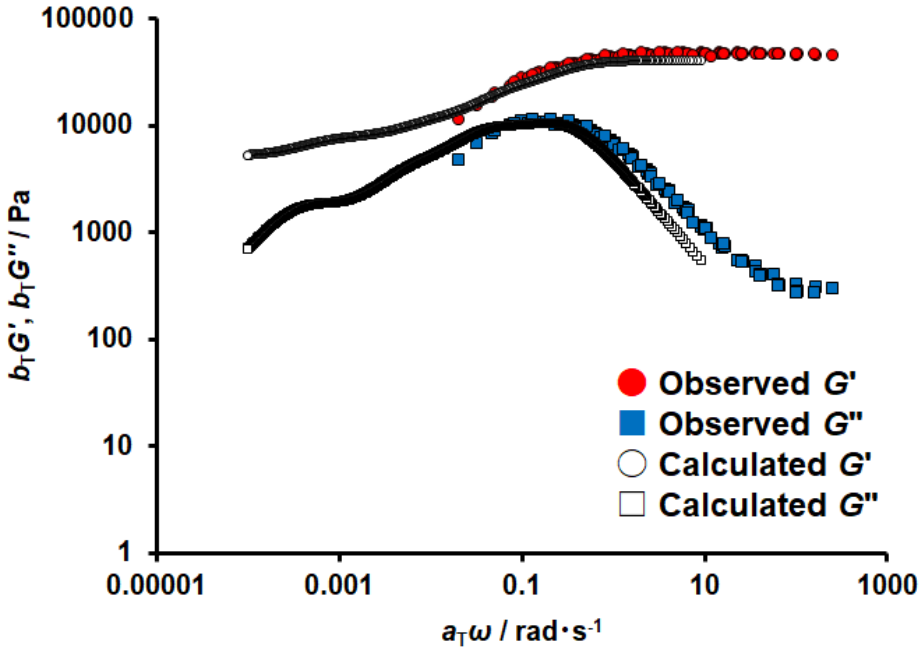

Figure S55. The comparison between calculated moduli and master curves of G' and G'' of the αCD-PyC11 hydrogel.

Calculated τ, $<\tau>_w$ and ΔE_a were summarized in **Table S11**. $<\tau>_w$ increased with increasing RESP fitted charge. On the other hand, ΔE_a was almost the same among the αCD-ImC11, αCD-PyC11, αCD-VC11 hydrogels. ΔE_a is one of the measure of the temperature dependence of the relaxation, which is not the life time of the stickers. These results suggest that the life time of the stickers is determined by the RESP fitted charge, resulting in the direct effect on the viscoelastic relaxation time. Noted that ΔE_a of the αCD-C12 hydrogel was higher than the others, which is attributed to the fact that the αCD-C12 hydrogel was turbid.

Table S11. Relaxation time (τ), second-order average relaxation times ($<\tau>_w$) and apparent activation energy (ΔE_a) of the αCD-R hydrogels.

	αCD-C12 hydrogel	**αCD-ImC11 hydrogel**	**αCD-PyC11 hydrogel**	**αCD-VC11 hydrogel**	**αCD-TMAmC11 hydrogel**
τ	n/a (< 0.01 s)	0.10 s 1.9 s	2.2 s 19 s	5.3×10^3 s	9.5×10^3 s
$<\tau>_w$	n/a	1.8 s	18 s	6.6×10^3 s	9.5×10^3 s
ΔE_a	84 kJ/mol	59 kJ/mol	63 kJ/mol	61 kJ/mol	92 kJ/mol

10. References

1 Y. Takashima, K. Otani, Y. Kobayashi, H. Aramoto, M. Nakahata, H. Yamaguchi and A. Harada, *Macromolecules*, 2018, **51**, 6318–6326.

2 Y. Takashima, Y. Sawa, K. Iwaso, M. Nakahata, H. Yamaguchi and A. Harada, *Macromolecules*, 2017, **50**, 3254–3261.

3 H. Yamaguchi, R. Kobayashi, Y. Takashima, A. Hashidzume and A. Harada, *Macromolecules*, 2011, **44**, 2395–2399.

4 H. Aramoto, M. Osaki, S. Konishi, C. Ueda, Y. Kobayashi, Y. Takashima, A. Harada and H. Yamaguchi, *Chem. Sci.*, 2020, **11**, 4322–4331.

5 W. Herrmann, B. Keller and G. Wenz, *Macromolecules*, 1997, **30**, 4966–4972.

6 Y. Kashiwagi, T. Katashima, M. Nakahata, Y. Takashima, A. Harada and T. Inoue, *J. Polym. Sci. Part B Polym. Phys.*, 2018, **56**, 1109–1117.

7 L. Leibler, M. Rubinstein and R. H. Colby, *Macromolecules*, 1991, **24**, 4701–4707.